

Hourly maximum individual wave height in the Indian shelf seas - its spatial and temporal variations in recent 40 years

Sanil Kumar V*, Jesbin George, Duphrin Joseph

Ocean Engineering, CSIR-National Institute of Oceanography (Council of Scientific & Industrial Research), Dona Paula, Goa - 403 004 India
Correspondance to email: sanil@nio.org

Abstract

The spatial and temporal variability of the high individual wave heights, which pose a hazard in India's shelf seas, has not been investigated. In this study, the spatial and temporal variation of hourly maximum individual wave height (H_{\max}) in the Indian shelf seas is examined based on 40 years ERA5 Re-Analysis data from European Centre for Medium-Range Weather Forecasts. Waverider buoy data from five locations are used to assess ERA5 H_{\max} . Variability of H_{\max} in different temporal scales; daily, monthly and interannual and their linkages with major ocean-atmosphere coupled interaction in the Pacific and the Indian Ocean are presented. Wave climatology throughout India's western shelf seas shows average H_{\max} exceeding 2m during most of the year. Maximum H_{\max} in the western shelf seas is during May-July, whereas in the southern tip and the eastern shelf seas are during the tropical cyclones and are either in October-December or May. Maximum H_{\max} is 17.94m and it occurred at the northern Bay of Bengal on 25 May 2009 during the passage of tropical cyclone Aila. Spatial variations in H_{\max} between locations spaced at 1.5° latitude are less than 10% in the northwestern and southeastern shelf seas, but large variations ($\sim 28\%$) are in the southwestern and northeastern shelf seas. Annual mean H_{\max} shows contrasting trends when data for 1979 to 2018 and 1992 to 2018 is considered. Indian Ocean Dipole influence on the H_{\max} suggests negative correlations in the western shelf seas and positive correlations in the eastern shelf seas. The correlation with climate indices is similar for both significant wave height and H_{\max} .

Keywords: climate indices, maximum wave height, north Indian Ocean, reanalysis data, surface waves, wave climatology .

1. Introduction

Ocean surface waves have a significant role in planning activities in the coastal zones and offshore areas (Tucker and Pitt 2001). The response of the waves to atmospheric forcing is complex since waves in the oceans compose wind-seas generated locally and remotely generated swells. Mainly the information on waves is obtained through, i) visual observations, ii) in situ measurements by wave buoys or satellite altimeter, iii) wave hindcast model (Cavaleri and Sclavo 2006). The data from the wave buoys are sparse and the spatial availability of the data is limited. In contrast, the data from the altimeters onboard satellite covers spatially large areas, but the temporal resolution (~ 10 days) is poor (Cooper and Forristall 1997). The wave hindcast model datasets have excellent spatial and temporal coverage, but the coarse resolution might not replicate the actual wave conditions. Data at larger time scales (> 3 h) underestimate the maximum value of significant wave height (H_s) by 6 to 26% during the monsoon and storm events (Anoop et al. 2014). Reanalysis gives the recent climate description by combining models with satellite altimeter data. Reanalysis data, especially from European Centre for Medium-Range Weather Forecasts (ECMWF), are now extensively used in climate studies in global and regional scales (Aarnes et al. 2014; Anoop et al. 2015). Recently, ECMWF released a new climate reanalysis data (ERA5), which is the 5th generation atmospheric reanalyses of the global climate (Hersbach and Dee 2016). ERA5 provides hourly data on a 31 km grid of a large number of climate variables related to the atmosphere and ocean.

For practical applications, like designing the air gap for offshore platforms and fixing the top level of the berthing structures, the value of the maximum height of an individual wave (H_{max}), i.e., the largest single one wave in a record (say 20 to 30 minutes), at a given place is required. Large wave heights also pose dangers to coastal and offshore infrastructure. Statistics on H_{max} can be derived from long historical records of hourly wave measurements. Numerical wave models or historical records provide values for H_s and hence, most of the studies based on wave models describe the variations in the bulk wave parameters such as; H_s , mean wave direction and wave period of wind sea and swell and do not describe the H_{max} (Aarnes et al. 2014; Amrutha et al. 2016; Sandhya et al. 2014; Semedo et al. 2011), except the recent study by Barbariola et al. (2019) and Naseef and Kumar (2020). When H_{max} is not known, generally, it is taken as 1.8 times the H_s (Goda 2000). The ERA5 data contain the information on H_{max} and recently, Naseef and Kumar (2019) studied the climatology of H_{max} in the Indian Ocean. All other reanalysis data sets like ERA-40, ECMWF Reanalysis Interim (ERA-Interim), National Centers for Environmental Predictions (NCEP)-Climate Forecast System Reanalysis (CFSR) do not contain H_{max} data.

The Indian Ocean monsoons are strong ocean-atmosphere interaction over the north Indian Ocean (NIO) during June-September. The wave heights, especially in the Arabian Sea (AS) and northern Bay of Bengal (BoB), are much higher during this period compared to the rest of the year (Naseef and Kumar 2020; Sanil Kumar and Anoop 2015). Hence, it is important to examine the H_{\max} during the monsoon period. Similarly, NIO is frequented by tropical cyclonic storms and the impact of these storms is higher in the BoB than in the AS (Singh et al. 2000). The tropical cyclones generate higher wave heights at a location for a shorter period of 3 to 5 days (Amrutha et al. 2014) and these higher wave heights pose a significant threat to the coastal areas. Waves generated by tropical cyclones dominate the extreme wave climate of the BoB and the waves generated in the Southern Hemisphere characterize swell waves in the NIO (Amrutha et al. 2017). Hence, the wave climate of the NIO consists of swells from the Southern Hemisphere as well as the locally generated wind waves and is influenced by a number of factors including the monsoon, tropical cyclones and large scale ocean-atmosphere coupled phenomena (Anoop et al. 2016; George et al. 2019; Hemer et al. 2010; Naseef and Kumar 2020).

Large-scale changes in waves in the nearshore are of critical importance for coastal engineers and scientists. The influence of climate indices on waves in the Indian Ocean was previously reported. For example, Hemer et al. (2010) observed that the Southern Annular Mode influences wave climate variability in the Indian Ocean. Lopez and Kirtman (2016) identified El Niño–Southern Oscillation (ENSO) as a potential source of wave height variability in the Indian Ocean. During El Niño events, Shukla et al. (2018) observed negative wave height anomaly over the BOB. During the NE monsoon period, Anjali Nair et al. (2019) reported that during strong El Niño years, the seasonal average wave height is relatively low in the northwestern BoB.

Changes in wave climate are quantified through trend estimation of wave height. All of the studies on long-term trend analysis describe the variations in the bulk wave parameters and do not describe the H_{\max} (Gulev and Grigorieva 2004; Semedo et al. 2011; Young et al. 2011) except the recent studies by Naseef and Kumar (2020), which examined the climatology and trend of waves in the Indian Ocean and the study by Barbariola et al. (2019), which analysed the characteristics of the maximal wave heights over the world oceans during 25 years (1992–2016) through combined numerical wave model outputs and extreme statistics. With the increase in sea surface temperatures (SST) and increased potential intensity, stronger TCs are expected (Emanuel 1988), which can lead to high H_{\max} . Motivated by these aspects, the present study examines the H_{\max} at 19 locations in the Indian shelf seas (Fig. 1) in the recent 40-years (1979 to 2018). Locations spaced $\sim 1.5^\circ$ latitude are selected. The data is also compared with available buoy measured data at five coastal locations in the

NIO. The details of the locations and the periods of the data used in the analysis are presented in Table 1. The waves during the monsoon and the tropical cyclone are also examined. The remainder of the paper is arranged as follows. The buoy data, ERA5 reanalysis, the method of the study and the ERA5 performance evaluation are shown in Section 2. Section 3 presents the results and discussion is in section 4. The paper ends in Section 5 with concluding remarks.

2. Data and method

2.1 ERA data

The study is based on the hourly maximum individual wave height (H_{\max}) parameter obtained from ERA5 Re-Analysis data of ECMWF. The ERA5 assimilation system uses the latest version of the Integrated Forecasting System (IFS Cycle 41r2) and modern parameterization technique of earth process which allows to use variational bias scheme for not only satellite observation, but also for aircraft, ozone and surface pressure data. The ERA5 data contains one (31 km) high-resolution realisation and a reduced resolution ten-member ensemble (Hersbach and Dee 2016). The present version of the ECMWF wave prediction system has a spatial resolution of 28 km, while the spectrum is discretized with 36 directions and 36 frequencies with starting frequency at 0.035 Hz (ECMWF 2019). Reanalysis data assimilate altimeter H_s into the product, starting in 1992. Based on the theory of wave-wave interaction, the height of the expected highest individual wave within a 20 minute time window (H_{\max}) is calculated from the wave spectrum. The calculation of H_{\max} is based on the work of Mori and Janssen (2006) for the determination of the time extreme. The H_{\max} distribution is obtained by simply writing down the probability that for a given number of waves, the H_{\max} has a certain chosen value. The climate at different locations is computed from the 40-year mean of the reanalysis from January 1979 to December 2018. The trend is the temporal linear changing rate of H_{\max} over 40 years.

2.2 Buoy data

The H_{\max} data measured using the Datawell directional waverider buoy is compared with ERA5 wave data. The locations and the period of data used for the comparison are presented in Table 1. The directional waverider buoy is neutrally buoyant and tracks the free surface and measure wave height using accelerometers. The buoy measures surface gravity waves with heaves in the range of -20 and +20 m, with a resolution of 1 cm in heaves and a range of wave periods between 1.6 and 30 s. Data recorded continuously at an interval of 1.28 Hz, and the data for every 30 min are processed as one record. The H_{\max} is the maximum wave height in a 30-minutes duration and is obtained from the

zero-crossing analysis of the surface elevation time series. From the measured data, the records at 1-hour intervals are utilized for comparative study with the ERA5 data.

2.3 Wave height distribution functions

The commonly used distribution functions listed below are fitted to the wave height distribution.

$$\text{Log-normal distribution function, } f(x) = \frac{\exp\left(-\frac{\log(x) - m^2}{2\sigma}\right)}{\sqrt{2\pi\sigma x}}, \quad x \geq 0 \quad (1)$$

Where, m and σ are mean and variance of $\log(x)$

$$\text{Rayleigh probability density function, } f(x) = 1 - \exp\left(-\frac{x^2}{2b^2}\right), \quad x \geq 0, b > 0, \quad (2)$$

Where b is the parameter of the distribution

Generalized Extreme Value Distribution is defined by the equation,

$$f(x) = \exp\left(-\left[1 + \beta\left(\frac{x - \mu}{\sigma}\right)\right]^{\frac{-1}{\beta}}\right), \quad \sigma > 0, 1 + \beta(x - \mu)/\sigma > 0 \quad (3)$$

Where β , μ and σ represents the shape, location, and scale parameters of the distribution function. The method of Probability Weighted Moments is used to estimate the distribution function.

2.4 Comparison of ERA5 with measured data

In this section, the ERA5 H_{\max} data is compared with the measured buoy data. The parameters used for comparison of the ERA5 H_{\max} data with the measured wave data are the root-mean-square error (RMSE), correlation coefficient (r), scattering index (SI) and bias, as defined below. The bias signifies the average difference between the ERA5 and buoy data and low RMSE values indicate a better fit of ERA5 data with measurements.

$$\text{RMSE} = \sqrt{\frac{1}{N} \sum_{i=1}^N (A_i - B_i)^2} \quad (4)$$

$$\text{Bias} = \frac{1}{N} \sum_{i=1}^N (A_i - B_i) \quad (5)$$

$$SI = \frac{\sqrt{\frac{1}{N} \sum_{i=1}^N [(A_i - \bar{A}) - (B_i - \bar{B})]^2}}{\bar{B}} \quad (6)$$

$$r = \frac{N \sum_{i=1}^N A_i B_i - \sum_{i=1}^N A_i \sum_{i=1}^N B_i}{\sqrt{\left[N \sum_{i=1}^N A_i^2 - \left(\sum_{i=1}^N A_i \right)^2 \right] \left[N \sum_{i=1}^N B_i^2 - \left(\sum_{i=1}^N B_i \right)^2 \right]}} \quad (7)$$

Where A_i represents the data obtained from the ERA5, B_i represents the data from the buoy measurements with N number of data points. Overbar represents the mean value.

The annual maximum value of H_{\max} at Ratnagiri from the ERA5 is 7.6 m, whereas the buoy measured data is 8.6 m, indicating an underestimation (~12%) in the ERA5 data (Fig. 2). Monthly maximum H_{\max} values are underestimated in ERA5 by 2 to 34%. At Karwar, the monthly maximum H_{\max} is underestimated by 2 to 10% in some months and overestimated by 2 to 20% in some months (Fig. 2). The annual maximum H_{\max} at Karwar from ERA5 is 6% less than the buoy measured value (Table 2). Whereas, in the western BoB at all the 3 locations, overestimation (3 to 25%) in annual maximum H_{\max} is noted in the ERA5 data (Table 2). The annual mean H_{\max} from ERA5 at all locations is higher (17 to 54%) than the buoy data. In order to examine the accuracy of the ERA5 during high sea states, the time series of buoy measured and ERA5 H_{\max} during peak monsoon at Ratnagiri and during TC Phailin at Gopalpur is compared (Fig. 3). The comparison statistics indicate that the H_{\max} is overestimated in ERA5 with RMSE of 0.69 m and 0.84 m during high monsoon and tropical cyclones, respectively (Table 2). One reason for the overestimation in ERA5 data is due to the fact that the ERA5 data grid point is a deeper water depth compared to the buoy location (Table 1). Wave data in ERA-5 were produced on a grid with a resolution of the order of 31 km, whereas the measured data is a point measurement. Even though shallow water physics is active in the model, due to the coarseness of the grid, the coupled-wave component (Janssen 2004) is coarser at approximately 31 km and the mean water depth at the point of interest is different from the buoy location (Table 1). Also, the data used for evaluating the ERA-5 data in the present study were collected using buoys located 1.5 to 5 km from the coast (Table 1). But the maximum H_{\max} of 13.5 m during the TC Phailin is slightly (4%) underestimated in ERA5 (12.95 m). These comparisons demonstrate that ERA5 H_{\max} reproduces mean and maximum values in Indian shelf seas within the reasonable biases.

3. Results

3.1 Monthly variations

Spatial distribution of the monthly average H_{\max} indicates that the Indian shelf seas have low values of H_{\max} (< 1 m) from January to April and from November to December except at the southern tip, where the wave heights are slightly higher (Fig. 4). From June to August, the wave heights in AS is higher than in the BoB. The highest monthly average H_{\max} is 6.9 m and is in July at $16-17^{\circ}$ N; $65-66^{\circ}$ E followed by 6.1 m in June and 5.5 m in August and is due to the influence of Findlater jet (Anoop et al. 2015). Lowest wave heights are from February to April, with a monthly maximum H_{\max} of 2.9 m.

Monthly maps of H_{\max} in the western shelf seas (locations 1 to 10) reveal a clear seasonal cycle with higher waves occurring during the SW monsoon (Fig. 5). The SW monsoon average H_{\max} is more than 3.5 m at all locations in the western shelf seas except at location 9, where the mean value is low (~ 2.8 m) due to the shadow effects of the Lakshadweep islands. Daily variation in H_{\max} during a year is examined by selecting 2018. The daily variation in H_{\max} during 2018 ranged from 0.01 to 5.55 m, with the mean value ranging from 0.29 to 0.58 m at different locations (Fig. 6). The maximum daily variation of 5.55 m is at location 16 on 17 December 2018 and this large variation is due to the severe cyclonic storm Phethai in the BoB. The monthly average H_{\max} is high in July in almost all the locations except at locations 12 to 15 and 18 (Fig. 7). The minimum of the monthly average H_{\max} for all locations in India's western shelf seas occurs in November-December, except at location 11 (Fig. 7). At locations 11 to 14, the monthly average H_{\max} is minimum in March, at locations 15 to 17, the minimum H_{\max} is in February and at 18 and 19, it is in January. The Coefficient of Variation (CV), namely the ratio between the standard deviations and the means, is low (~ 0.31) for locations 11, 14 and 15, indicating the low variability in wave height. In contrast, CV is high (~ 0.58) at locations 1 to 3.

The maximum value of H_{\max} in the Indian shelf seas in different years varied from 6.72 m (location 11) to 17.94 m (location 19). The maximum H_{\max} from 1979 to 2018 is 17.94 m and it occurred on 25 May 2009 at the northern BoB (location 19) during the passage of tropical cyclone Aila. The maximum H_{\max} in India's western shelf seas is 15.99 m and it occurred at location 2 on 8 June 1998 at the northeastern AS during the cyclonic storm ARB02 (Table 3). At all the AS locations, the maximum H_{\max} occurred between May and July except at the southernmost point in AS. At all the locations in the BoB, the maximum H_{\max} is either during October-December or in May and is during the tropical cyclones (Table 3).

3.2 Annual cycle and inter-annual variations

The annual mean H_{\max} at different locations in the eastern AS varied from 1.87 (location 9) to 2.94 m (location 11), whereas the annual mean H_{\max} at locations in the western BoB is 1.60 (location 15) to 2.49 m (location 19) (Fig. 8 & Table 4). Large interannual variations are observed in the annual maximum value of H_{\max} from 1979 to 2018 at all the locations due to the influence of storm/tropical cyclone (Fig. 9). In contrast, the inter-annual variations in annual mean H_{\max} are less (Fig. 10) since the influence of tropical cyclones on the wave at a location lasted only for 3 to 4 days. The mean value of annual maximum H_{\max} at different locations varies from 4.95 (location 9) to 8.38 m (location 2) in the eastern AS and from 4.90 (location 12) to 8.91 m (location 19) in the northern BoB (Table 4). The northern BoB is the region where intense tropical cyclones make their landfall and hence, the mean value of the annual maximum H_{\max} from 1979 to 2018 is maximum in this region. In contrast, the mean of the annual mean from 1979 to 2018 is less in the northern BoB (2.49 m) compared to the southern location (2.94 m) and the eastern AS (2.60 to 2.67 m). The annual average H_{\max} in a year had the highest value (3.11 m in 1995) at location 11 and the lowest (1.50 m in 1998) is at location 15.

The annual averages of the H_{\max} and the annual maximum, the 95th and 99th percentiles of H_{\max} from 1979 to 2018, are plotted in Fig. 8. High waves are present and the higher values (95th percentile) in particular are noticeable throughout the year. The 99th, 95th and 90th percentile and annual mean values are minimum at location 15 and maximum at location 2. The 99th percentile H_{\max} varied from 3.2 m to 7.0 m with an average value of 5.3 m, whereas 95th percentile values ranged from 2.4 to 5.9 m and the 90th percentile ranged from 2.2 to 5.2 m with an average value of 3.8 m. Annually, in the western shelf seas at locations 1 to 5, H_{\max} more than 4 m occurred during 18 to 20% of the time, whereas in the eastern shelf seas, it is less than 5% of the time, except at location 19. Similarly, H_{\max} more than 8 m is during 0.1 to 0.2% of the time in locations 1 to 7 the western shelf seas and location 19 in the eastern shelf seas (Table 3). Among the locations studied, the 75th, 50th and 25th percentiles of H_{\max} is highest at location 11, indicating that at this area, low wave heights are less.

3.3 Abnormality index

The abnormality index, i.e., the H_{\max} to H_s ratio, varied from 1.72 to 2.10, with a mean value of 1.89 at different locations. When H_{\max} is more than two times the corresponding H_s , the wave is called as freak waves (Mori and Janssen 2006). On average, annually, freak waves occurred 0.1% the time in the study area with maximum (0.7%) at location 15. Most of the time, the abnormality index

varied from 1.6 to 2. The comparison of the abnormality index obtained from ERA5 with the buoy measurements indicates that the ERA5 values are high. Annually, the abnormality index from buoy measurements varies from 1.71 to 1.73, whereas the same from ERA5 data is 1.88 to 1.90 (Table 2). Also, the value of the abnormality index during the high waves at Ratnagiri and TC Phailin is 1.67, whereas that from ERA5 is 1.84 to 1.88 (Table 2). The theoretical value of the abnormality index is 1.62 to 1.64 for 190 to 220 waves (Longuet-Higgins, 1952). Kumar et al. (2020) observed that during the TC Hudhud, the ratio between H_{\max} and H_s for the 30 minutes measured buoy data at a location in the Bay of Bengal varied from 1.4 to 2.3, with an average value of 1.66.

3.4 Wave height distribution

The comparisons between the histograms of H_{\max} and the theoretical distributions, i.e., log-normal and GEV distributions, are presented in Fig. 11. The theoretical wave height distributions do not show a good fit in the case of rapidly changing wave conditions similar to that at locations 1 to 7. The rapidly changing wave conditions at these locations are due to SW monsoon and the distributions were not able to pick up these variations. All the distributions underestimate the peak of the histograms (Fig. 11) for locations 1 to 7. Log-normal and GEV distributions produce a more accurate fit for those locations (locations 13 to 16) with exponential increase and decrease in wave height and comparatively low fit for locations with irregular distribution of wave heights. The most frequent high values occur at locations 1 to 7, whereas low values are least at location 11. The wave height distribution is narrow at locations 13 to 15. When the range of wave heights is too broad, the log-normal and GEV distributions show a slight shift from the peak values (locations 17 and 18). Also, the distributions are under-predicting for locations in the AS. For the locations from 17 to 19, the graphs are broad and have no sudden peak. In these cases, the log-normal and GEV distributions slightly under predicts the maximum values but gives a good estimation than Rayleigh distribution. Location 11 situated off the southern tip of India has the highest annual mean H_{\max} and lowest highest H_{\max} during the 40 years among the locations studied, indicating that the variability is least at this location. This location has no sudden peak or sudden decrease in the distribution of H_{\max} and the frequency of occurrence is almost the same for the range of 2 to 3m.

To further examine the fit of the distributions, RMSE is calculated for each location (Table 5). RMSE values for log-normal and GEV distributions are greater than 1 in locations 1 to 7 and Rayleigh distribution showed very high values ($RMSE > 2$). RMSE is less for locations in the BoB than in the AS. Compared to other distributions, log-normal distribution fits better for locations in the AS. The log-normal and GEV distributions are almost similar for the locations in BoB.

Comparing the fitted distributions and the RMSE values for the wave data at locations 13 to 16, we can see that the log-normal and GEV distribution could give an acceptable representation to the measured wave data with RMSE values less than 0.32 (Table 5).

3.5 Seasonal and annual anomalies

The earlier studies (Glejin et al. 2013; Anoop et al. 2015; Naseef and Kumar 2019) in the NIO indicate that the wave characteristics are different in 3 seasons; pre-monsoon (February-May), SW monsoon (June-September) and NE monsoon (October-January). Accordingly, the seasonal anomalies are calculated relative to the seasonal climatology (e.g., SW monsoon anomaly is relative to the average of all SW monsoon for the 40-year) (Fig. 12). The annual anomaly in H_{\max} varied from -0.24 to 0.25 m, whereas the seasonal anomaly during the pre-monsoon period varied from -0.33 to 0.37 m and that during the SW monsoon varied from -0.59 to 0.64 m (Fig. 12). The seasonal anomaly during the NE monsoon varied from -0.33 to 0.43 m. The differences between the mean and maximum values of H_{\max} are more for most of the locations, as a result of the marked seasonality of the waves in the study area. Seasonally, in the western shelf seas, SW monsoon waves are the largest (mean = 3.9 m) and most variable, whereas NE monsoon waves are the smallest (mean = 1.7 m) and least variable. In the eastern shelf seas, SW monsoon waves are lower than in AS with a mean value of 2.4 m, while in the pre-monsoon seasonal mean H_{\max} is 1.8 m. During the NE monsoon, both in the western shelf seas and eastern shelf seas average seasonal H_{\max} is 1.7 m. The study shows pronounced interannual variability along with a seasonal cycle. During the NE monsoon season, typically from October to January, the seasonal maximum H_{\max} can change from year to year by a factor of 5, especially in the northeastern shelf seas (locations 17 to 19) and this change is due to the tropical cyclones. In contrast, the year to year variation in the seasonal mean H_{\max} is only by a factor 1.2 to 1.4. During the SW monsoon, the year to year variation in the seasonal maximum H_{\max} is by a factor 1.3 to 2.4, while the variation in the seasonal mean H_{\max} is much less (1.2 to 1.3).

3.6 Spatial variation

The spatial variations in wave climate are examined by computing the relative differences of both the average of the annual mean H_{\max} and the average of the annual maximum H_{\max} between the two locations. Between locations 1 to 7, the variations in the average of the annual mean H_{\max} are within 7% and that in the average of the annual maximum H_{\max} is within 8%. Between the locations 8 to 10, a large difference (~28%) is observed due to the presence of the Lakshadweep Islands. The latitudinal variation in annual mean H_{\max} is 0.74 m in 3° and is highest between locations 7 and 9. Between locations 12 to 15, the variations in wave climate are within 10%. In contrast, between 15 to

19, large variations (~23%) is observed both in annual mean and annual maximum H_{\max} . From location 15 to 19, the annual mean H_{\max} increased from 1.6 m to 2.5 m and the annual maximum H_{\max} increased from 5.2 to 8.9 m. In the eastern shelf seas, the location 19 situated in the Head Bay of Bengal has higher extreme waves over the 40 years.

Along the west coast of the United States, the annual mean H_s varied from 2.1 to 2.3 m within 110 km indicating that the spatial variation in annual mean H_s is less than 10% (Altunkaynak and Özger 2018), which is similar to the variation observed in the present study between locations 1 and 7. Ashton et al. (2013) studied wave data from an array of four directional wave buoys installed at the four corners of a square with 0.5 km in the Celtic Sea, UK and reported that the annual mean value changed from 1.74 to 1.78 m Southwards and 1.74 to 1.76 m Eastwards in a span of 0.5 km.

3.7 Long-term trend

The 40-year long-term data, which is higher than the minimum (~30 years) recommended by the World Meteorological Organization to make reliable estimations of climate variables in a region (WMO, 1989), makes it possible to assess the interannual variability. At most of the locations, H_{\max} showed an overall increasing trend during the 40 years. The strongest positive trend in annual mean H_{\max} is found in the western shelf seas (0.17 to 0.44 cm/year), while the same trends in the annual maxima are rather spread across (Figs. 9 and 10). The trend in annual mean H_{\max} for the eastern shelf seas varied from 0 to 0.22 cm/year, while the trend in annual maximum varied in large range due to the frequent tropical cyclones in the BoB and is from -1.7 cm/year (location 19) to 4.6 cm/year (location 17) with the mean trend of 1.1 cm/year. The 99th percentile of H_{\max} showed -0.1 (location 15) to 1.4 cm/year (location 7) with a mean trend of 0.75 cm/year. The average trend in the 95th and 90th percentile of H_{\max} is 0.7 and 0.6 cm/year (Table 4). The annual maximum H_{\max} trend is slightly higher than the annual maximum H_s trend (Table 4).

Aarnes et al. (2015) reported that combining years before and after 1992 may not provide a meaningful trend in wave parameters due to the assimilation of altimeter wave heights into the reanalysis products starting in 1992. In order to examine the difference in trend from 1979 to 1991 and from 1992 to 2018, the trend of annual mean H_{\max} during both periods is estimated and presented in Fig. 10. The average trend in annual mean H_{\max} from 1992 to 2018 in the study area varied from -0.68 to 0 cm/year with a mean value of -0.35 cm/year, whereas for the period before 1992, it varied from 0.1 to 1.4 cm/year. When full data (1979 to 2018) is considered, H_{\max} showed an overall increasing trend. Similarly, the 99th percentile of H_{\max} also showed a negative trend with a mean value of -0.30 cm/year when 1992 to 2018 data is considered.

3.8 Relations to climate indices

Wave climate of the NIO is mainly influenced by two major ocean-atmosphere coupled phenomena; one in the Pacific Ocean, i.e., El Niño – Southern Oscillation (ENSO) (Schott et al. 2009) and another in the Indian Ocean i.e., Indian Ocean Dipole (IOD) (Anoop et al. 2016; Fu et al. 2018). Here we have examined the relationship of these two modes of climate variability with H_{\max} along Indian Shelf seas. Figure 13a shows the correlations coefficients (R) of H_{\max} anomalies along 19 locations during pre-monsoon, SW monsoon and NE monsoon seasons with annual averaged Oceanic Niño Index (ONI). During pre-monsoon, R values range from -0.44 to 0.15 with strong negative correlations observed along location 11, followed by location 12, whereas a positive correlation is observed along location 15. Interestingly all the locations along the Indian shelf seas, except location 15, show negative correlations with ONI. However, during NE monsoon, the R values weaken (-0.2 to 0.2) with most locations showing a weak as well as strong negative correlations and few locations shows strong to weak positive correlations. During SW monsoon, a strong to weak negative correlations (R ranges from -0.19 to -0.05) were observed along the locations in the AS whereas, weak to strong positive correlations (R ranges from 0.06 to 0.38) in the locations along BoB. The R values along the BoB is observed to be stronger in comparison with R values along AS during SW monsoon. Maximum negative correlations are observed along location 8, followed by location 9 and maximum positive correlation is along location 13, followed by location 12. In general, during pre and NE monsoon seasons, most locations give weak, as well as strong negative correlations, whereas a few locations show weak positive correlations. But during the SW monsoon, shelf regions of AS show negative correlations and shelf regions of BoB show positive correlations.

Fig. 13b shows the correlations coefficients of H_{\max} anomalies observed during October with the dipole mode index (DMI). The month of October was chosen, as the significant wind anomalies induced by IOD peaks during this month (Anoop et al. 2016). The H_{\max} during October is significantly negatively correlated along the locations of the Arabian Sea with DMI (Fig. 13b). The R values with DMI and H_{\max} along AS ranges from -0.24 to -0.47, with the strongest correlation, observed along the location 6 and the weakest one along location 1. In contrast, positive correlations are observed in the BoB locations (12-15, ranging from 0.06 to 0.26) and strong negative correlations in the rest of the locations (R ranging from -0.19 to -0.38).

4. Discussion

The maximum ERA5 H_{\max} data during the TC Phailin is lower (4%) than that of the measured buoy data. This is consistent with the earlier observation of 2.7% underestimation in ERA5 H_s (Naseef and Kumar, 2020) during the tropical cyclone. Buoy data appear valid up to 10% of wave height (Jensen et al. 2015), so the difference of less than 10% is virtually identical. It also may be less important that the ERA5 data is off when H_{\max} is small.

The earlier measured maximum value of H_{\max} in the NIO is 13.5 m at 50 m water depth off Gopalpur during TC Phailin in 2013 (Amrutha et al. 2014). During TC Thane on 29 December 2011, H_{\max} of 8.1 m is measured off Puducherry (Kumar et al. 2013). Along the west coast of India, H_{\max} of ~10.1 m is reported during a storm in 1996 at 23 m water depth (Kumar et al. 2006). The present study indicates that H_{\max} up to 15.99 m and 17.94 m can occur in India's western and eastern shelf seas. But the maximum H_{\max} in the Indian shelf areas is less than that in the Southern Ocean (H_{\max} ~ 23.8 m) and North Atlantic Ocean (27.3 m) (Naseef and Kumar 2020). Whereas, the maximum H_s measured in the eastern and western shelf seas is 7.3 m (Amrutha et al., 2014) and 5.1 m (Kumar et al., 2000). Even though H_{\max} is the maximum value during the 30 minutes period and H_s is the average of the highest one-third of the waves in that 30 minutes, the climatology and seasonal variations of H_{\max} is similar to that of H_s , but with a higher magnitude, i.e., 1.89 times the H_s .

The comparisons between the histograms of H_{\max} and the theoretical distributions show that both log-normal and GEV distributions fit better than the Rayleigh distribution. The theoretical wave height distributions do not show a good fit for locations having rapidly changing wave conditions. Wave conditions at location 11 are different from others due to the presence of Sri Lanka has a very broad range of H_{\max} values and the distributions did not show good fit in the tail ends as well as at the peak. Li et al. (2016), Teng and Palao (1996) and Dong et al. (2013) reported a good fit for log-normal distributions for H_s in various locations around the globe.

The trend presented from 1979 to 2018 is to be looked at with caution. Naseef and Kumar (2020) reported the average trend in annual mean H_s and maximum H_s from 1991 to 2017 in the Indian Ocean is -0.07 and -0.64 cm/year, respectively. The decreasing trend in H_{\max} observed in the present study is similar to the decreasing trend in H_s reported by Naseef and Kumar (2020). Also, Aarnes et al. (2015) showed that there is a decrease of H_s (0-0.5% of the annual mean value per year) from 1992 - 2012. The warmer seas produce extreme events like more tropical cyclones in Arabian Sea and Bay of Bengal. But the track of TC is not always the same. The maximum H_{\max} observed at most of the locations are due to different TCs (Table 3). The TC generated H_{\max} also varies

significantly within 300 km distance based on the characteristics of TC. During TC Phailin, on 12 October 2013, the H_{\max} at locations 17 and 18 spaced ~ 289 km is 11.59 and 12.49 m, whereas during TC Hudhud, on 12 October 2014, it is 12.67 and 7.88 m, respectively. Similarly, during the TC Hudhud, on 12 October 2014, the wave rider buoys in western Bay of Bengal located at Gangavaram and Gopalpur spaced at a distance of ~ 260 km recorded H_{\max} of 10.5 and 9.2 m. Also, for locations 1 to 7 (eastern Arabian Sea), the strongest TC were from 1989 to 1999 (Table 3). In the linear trend estimate, few peak values can alter the trend. Hence, the trend reported here is to be used with caution. Recently Lin and Oey (2020) reported that regions dominated by younger waves have an increasing trend in H_s and wind trends and areas dominated by older waves have a decreasing trend in H_s . Since the Indian shelf seas is a swell dominated region with swells from the south Indian Ocean and the Southern Ocean (Stopa and Cheung 2014, Naseef and Kumar 2020), the decreasing trend in H_{\max} observed is in agreement with the observation of Lin and Lin and Oey (2020) for H_s . The study results emphasize that the reanalysis data has to be used with caution for long-term trend analysis because the quality of the data being assimilated changes in time (Stopa et al. 2019).

A strong to weak positive and negative correlation is observed with H_{\max} anomalies and ONI along different locations in the Indian shelf seas, particularly during pre and NE monsoon. Shukla et al. (2018) also observed similar negative (positive) anomalies in the Indian Ocean, but based on H_s anomalies, during January and May and are linked with El Niño (La Niña) events. The H_{\max} along the NIO decreases (increases) since the trade winds along the equatorial Indian Ocean weakens (strengthens) during El Niño (La Niña) events (Taschetto et al. 2011). But during the SW monsoon, weak negative correlations were observed along the locations in the AS whereas, strong positive correlations in the locations along BoB. The extreme waves generated in the mid-Indian Ocean during the negative phase of ENSO (Izaguirre et al. 2011) propagates to the NIO in an east-northeastward direction and as a result, more swells propagates to BoB than to the AS (Sabique et al. 2012). The observed weak positive correlations in the BoB might be due to the resultant effect of mid-Indian Ocean extreme waves reaching the BoB. But the south-west BoB (locations 12-15), which shows a strong positive correlation, are influenced by the landmass (Sri Lanka), which acts as a shadow zone and reduces the H_{\max} along this region (Table 3). Wind-seas along this region play a vital role in determining the wave climate, which enhances during La Niña conditions resulting in a strong positive correlation. Izaguirre et al. (2011), based on satellite data, suggests that negative phases in ENSO (La Niña) and IOD increase extreme wave heights in the central Indian Ocean and the eastern Indian Ocean, respectively. In October, we observed significant negative correlations with DMI and H_{\max} in the AS and in contrast, positive correlations in the BoB, which are similar to

the previously reported negative and positive correlations in H_s anomalies with DMI in AS (Anoop et al. 2016) and BoB (Fu et al. 2018) respectively. The present study shows that the correlation with climate indices is similar for both H_s and H_{max} .

5. Summary and conclusions

The present work characterizes the seasonal and inter-annual variability of the maximum wave height at 19 locations around the Indian sub-continent based on ERA5 data from 1979 to 2018. The data is compared with in situ buoy measurements at 5 locations. The annual maximum value of H_{max} is slightly underestimated in the ERA5 data, but during the peak monsoon and Tropical Cyclone period, slight overestimation is observed. The abnormality ratio from ERA5 data is higher than that from the buoy measured values. After assessing the general characteristics and seasonality of the H_{max} , the possible trends in time are examined. The maximum H_{max} of 17.94 m in the shelf seas of India occurred at the northern Bay of Bengal on 25 May 2009 during the passage of tropical cyclone Aila. The variations up to 5.55 m are observed in the H_{max} in a day due to the severe cyclonic storms. The maximum H_{max} is from May to July in the AS, while at the southernmost point and at all the locations in the BoB, it is either during October-December or in May and is during the tropical cyclones. The seasonal maximum H_{max} can change from year to year by a factor of 5, especially in the northeastern shelf seas during the NE monsoon due to the tropical cyclones.

The spatial variations in waves between locations spaced at 1.5° latitude are less than 10% in the northwestern and southeastern shelf seas. In contrast, the variations are high ($\sim 28\%$) in the southwestern shelf seas due to the presence of the Lakshadweep Islands and in the northeastern shelf seas due to the tropical cyclones. The other aspect explored in this study is how the theoretical distribution fits the H_{max} distribution. The log-normal and GEV distributions fit well when the H_{max} showed a gradual increase and decrease and the H_{max} values are distributed within a short-range. Annually, 0.01 percentage of sea states are with an abnormality index of more than 2, resulting in freak waves. The trend estimate shows a positive trend in H_{max} while considering data from 1979 to 2018, while it becomes negative for data from 1992 to 2018. Hence, the reanalysis data has to be used with caution for long-term trend analysis due to the fact that the quality of the data being assimilated changes in time. The relationship between H_{max} and ENSO suggests weak negative correlations during pre and NE monsoon season for almost all the locations and weak positive correlations in some locations, which are associated with El Niño and La Niña events. However, during SW monsoon, strong positive correlations in BoB are associated with La Niña conditions.

IOD influence on the H_{\max} suggests a negative correlation in the AS and positive correlations in the BoB. The correlation with climate indices is similar for both significant wave height and H_{\max} .

Acknowledgments

The authors acknowledge the Council of Scientific and Industrial Research, New Delhi for funding the research work and Indian National Centre for Ocean Information Services (INCOIS), Ministry of Earth Sciences, for funding the wave measurement program as a part of the Ocean State Forecast for north Indian Ocean. ERA5 data used in this study have been obtained from the European Centre for Medium-Range Weather Forecasts data server: <http://data.ecmwf.int/data>. We thank all the reviewers and Associate Editor for the constructive comments and suggestions which improved the content of the paper. The authors thank Muhammed Naseef for helping with the ERA5 data. This publication is a NIO contribution xxxx.

References

- Aarnes OJ, Abdalla S, Bidlot J, Breivik Ø (2014) Marine wind and wave height trends at different ERA-Interim forecast ranges. *Journal of Climate* 28; 819-837doi: 10.1175/JCLI-D-14-004701
- Abdusselam A, Özger, M (2005) Spatial significant wave height variation assessment and its estimation. *Journal of Waterway Port Coastal and Ocean Engineering* 131: 277–282. 10.1061/(ASCE)0733-950X(2005)131:6(277)
- Amrutha MM, Sanil Kumar V, Jesbin George (2017) Observations of long-period waves in the nearshore waters of central west coast of India during the fall inter-monsoon period. *Ocean Engineering* 131: 244-262, 10.1016/j.oceaneng.2017.01.014
- Amrutha MM, Sanil Kumar V, Anoop TR, Balakrishnan Nair TM, Arun Nherakkol, Jeyakumar C (2014) Waves off Gopalpur, northern Bay of Bengal during the Cyclone Phailin. *Annales Geophysicae* 32: 1073-1083, doi:10.5194/angeo-32-1073-2014
- Amrutha MM, Sanil Kumar V, Sandhya KG, Balakrishnan Nair TM, Rathod JL (2016) Wave hindcast studies using SWAN nested in WAVEWATCH III - comparison with measured nearshore buoy data off Karwar, eastern Arabian Sea. *Ocean Engineering* 119: 114-124 10.1016/j.oceaneng.2016.04.032
- Anjali Nair M, Sanil Kumar V, Amrutha MM, Murty VSN (2019) Features of locally and remotely generated surface gravity waves in the inner-shelf region of north-western Bay of Bengal. *International Journal of Climatology* 39: 1644–1664 <https://doi.org/10.1002/joc.5907>
- Anoop TR Sanil Kumar V, Shanas PR (2014) Spatial and temporal variation of surface waves in shallow waters along eastern Arabian Sea. *Ocean Engineering* 81: 150-157, doi: 10.1016/j.oceaneng.2014.02.010

- Anoop TR, Sanil Kumar V, Shanas PR, Glejin Johnson (2015) Surface wave climatology and its variability in the North Indian Ocean based on ERA-Interim reanalysis, *Journal of Atmospheric and Oceanic Technology* 32: 1372-1385, doi: 10.1175/JTECH-D-14-002121
- Anoop TR, Sanil Kumar V, Shanas PR, Glejin Johnson, Amrutha MM (2016) Indian Ocean Dipole modulated wave climate of eastern Arabian Sea. *Ocean Science* 12: 369-378, doi:10.5194/osd-12-2473-2015
- Ashton IGC, Saulnier JB, Smith GH (2013) Spatial variability of ocean waves, from in-situ measurements, *Ocean Engineering* 57: 83-98. <http://dx.doi.org/10.1016/j.oceaneng.2012.08.010>
- Barbariola F, Bidlot J, Cavaleri L, Sclavo M, Thomson J, Benetazzo A (2019) Maximum wave heights from global model reanalysis, *Progress in Oceanography* 175: 139-160
- Cavaleri L, Sclavo M (2006) The calibration of wind and wave model data in the Mediterranean Sea. *Coastal Engineering* 53: 613–627
- Cooper CK, Forristall GZ (1997) The Use of Satellite Altimeter Data to Estimate the Extreme Wave Climate. *Journal of Atmospheric and Oceanic Technology* 14: 254–266
- Dong S, Wang N, Liu W, Soares CG (2012). Bivariate maximum entropy distribution of significant wave height and peak period. *Ocean Engineering* 59: 86-99, <https://doi.org/10.1016/j.oceaneng.2012.12.002>
- ECMWF (2019). IFS documentation CY43r1, Part VII: ECMWF wave model (ECMWF Model Documentation): European Centre for Medium-Range Weather Forecasts. <https://www.ecmwf.int/en/elibrary/19311-part-vii-ecmwf-wave-model> (accessed on 10 May 2020)
- Emanuel K (1988) The maximum intensity of hurricanes. *J. Atmos. Sci.*, 45, 1143–1155, [https://doi.org/10.1175/1520-0469\(1988\)045,1143:TMIOH.2.0.CO;2](https://doi.org/10.1175/1520-0469(1988)045<1143:TMIOH.2.0.CO;2).
- Fu C, Wang D, Yang L, Luo Y, Zhou F, Priyadarshana T, Yao J (2018) The relationship between significant wave height and Indian Ocean Dipole in the equatorial North Indian Ocean. *Ocean Dynamics* 68: 689–699 <https://doi.org/10.1007/s10236-018-1154-8>
- George J, Kumar VS (2019) Long-term variations in nearshore wave climate and littoral drift at Ganpatipule coast, eastern Arabian Sea and its link to Pacific climate variability. *Journal of Geophysical Research: Oceans*, 124: 7307–7327. doi: 10.1029/2018JC014900
- Goda, Y (2000) *Random Seas and Design of Maritime Structures*, 2nd ed, World Scientific, New Jersey, USA
- Gulev SK, Grigorieva V (2004) Last century changes in ocean wind wave height from global visual wave data. *Geophysical Research Letters* 31: L24302, doi: 10.1029/2004GL021040
- Hemer MA, Church JA, Hunter JR (2010) Variability and trends in the directional wave climate of the Southern Hemisphere. *International Journal of Climatology* 30: 475–491, <https://doi.org/10.1002/joc1900>
- Hersbach H, Dee D (2016) ERA5 reanalysis is in production *ECMWF Newsletter*, 147, 7

- Izaguirre C, Méndez FJ, Menéndez M, Losada IJ (2011) Global extreme wave height variability based on satellite data. *Geophysical Research Letters* 38: L10607, doi:10.1029/2011GL047302
- Janssen PAEM (2004) *The Interaction of Ocean Waves and Wind*. Cambridge University Press, Cambridge, UK, 312 pp.
- Jensen RE, Swail VR, Bouchard RH, Riley RE, Hesser TJ, Blaseckie M, MacIsaac C (2015) Field Laboratory for Ocean Sea State Investigation and Experimentation: FLOSSIE Intra-Measurement Evaluation of 6N Wave Buoy Systems. 14th International Workshop on Wave Hindcasting and Forecasting, November 2015, Key West, Florida USA; <http://www.waveworkshop.org>
- Kumar VS, Glejin J, Dubhashi KK, Nair TMB (2013) Waves during THANE cyclone, Bay of Bengal, *Natural Hazards*, 69, 509-522 doi 10.1007/s11069-013-0713-z
- Kumar VS, Pathak KC, Pednekar P, Raju NSN, Gowthaman R (2006) Coastal processes along the Indian coastline. *Current Science* 91(4): 530-536
- Kumar VS, Kumar KA, Anand NM (2000) Characteristics of waves off Goa, West coast of India, *Journal of Coastal Research* 16(3), 782-789. www.jstor.org/stable/4300088
- Kumar VS, Harikrishnan, Mandal S (2020) Wave crest height distribution during the tropical cyclone period, *Ocean Engineering* 197, 106899, doi.org/10.1016/j.oceaneng.2019.106899
- Lin Y, Oey L (2020) Global Trends of Sea Surface Gravity Wave, Wind, and Coastal Wave Setup. *J. Climate*, 33, 769–785, <https://doi.org/10.1175/JCLI-D-19-0347.1>
- Li W, Isberg J, Waters R, Engström J, Svensson O, Leijon M (2016) Statistical analysis of wave climate data using mixed distributions and extreme wave prediction. *Energies* 9(6), 396. <https://doi.org/10.3390/en9060396>
- Lopez H, Kirtman BP (2016) Investigating the seasonal predictability of significant wave height in the West Pacific and Indian Oceans. *Geophysical Research Letters* 43: 3451–3458. <https://doi.org/10.1002/2016GL068653>
- Mori N, Janssen PAEM (2006) On kurtosis and occurrence probability of freak waves. *Journal of Physical Oceanography* 36: 1471–1483
- Naseef TM, Sanil Kumar V (2020) Climatology and trends of the Indian Ocean surface waves based on 39-year long ERA-5 reanalysis data. *International Journal of Climatology* 40: 979-1006. doi.org/10.1002/joc6251
- Sabique L, Annapurnaiah K, Balakrishnan Nair TM, Srinivas K (2012) Contribution of Southern Indian Ocean swells on the wave heights in the Northern Indian Ocean - A modeling study. *Ocean Engineering* 43: 113-120, <https://doi.org/10.1016/j.oceaneng.2011.12.024>
- Sandhya KG, Nair TMB, Bhaskaran PK, Sabique L, Arun N, Jeykumar K (2014) Wave forecasting system for operational use and its validation at coastal Puducherry, east coast of India. *Ocean Engineering* 80: 64-72
- Sanil Kumar V, Anoop TR (2015) Spatial and temporal variations of wave height in shelf seas around India. *Natural Hazards* 78: 1693-1706, doi: 10.1007/s11069-015-1796-5

- Schott FA, Xie S-P, McCreary J P (2009) Indian Ocean circulation and climate variability. *Rev Geophys* 47: RG1002, doi:101029/2007RG000245
- Semedo A, Sušelj K, Rutgersson A, Sterl A (2011) A global view on the wind sea and swell climate and variability from ERA-40. *Journal of Climate* 24: 1461–1479, doi: 101175/2010JCLI37181
- Shukla RP, Kinter JL, Shin CS (2018) Sub-seasonal prediction of significant wave heights over the Western Pacific and Indian Oceans, part II: The impact of ENSO and MJO. *Ocean Modelling* 123: 1–15. <https://doi.org/10.1016/j.ocemod.2018.01.002>
- Singh OP, Khan TMA, Rahman S (2000) Changes in the frequency of tropical cyclones over the North Indian Ocean. *Meteorol Atmos Phys* 75: 11–20
- Stopa JE, Ardhuin F, Stutzmann E, Lecocq T (2019) Sea state trends and variability: Consistency between models, altimeters, buoys, and seismic data (1979–2016). *Journal of Geophysical Research: Oceans* 124: 3923–3940. <https://doi.org/10.1029/2018JC014607>
- Stopa JE, Cheung KF (2014) Intercomparison of Wind and Wave Data from the ECMWF Reanalysis Interim and the NCEP Climate Forecast System Reanalysis. *Ocean Modelling* 75: 65–83. <https://doi.org/10.1016/j.ocemod.2013.12.006>
- Taschetto AS, Gupta AS, Hendon HH, Ummenhofer CC, England, MH (2011) The contribution of Indian Ocean sea surface temperature anomalies on Australian summer rainfall during EL Niño events. *Journal of Climate* 24: 3734–3747, <https://doi.org/10.1175/2011JCLI38851>
- Teng CC, Palao IM (1996) Wave Height and Period Distributions From Long-term Wave Measurement, *Proceedings 25th International Conference on Coastal Engineering* 1(25). September 2–6, 1996, Florida, United States <https://doi.org/10.9753/icce.v25.%p>
- Tucker MJ, Pitt EG (2001) *Waves in Ocean Engineering* Elsevier New York, p 521
- WMO (1989) Calculation of monthly and annual 30-year standard normals, WMO/TD-No. 341, Tech rep World Meteorological Organization Geneva, Switzerland
- Young I R, Zieger S, Babanin A V (2011) Global trends in wind speed and wave height. *Science*, 332(6028): 451–455 <https://doi.org/10.1126/science.1197219>

1Table 1. Details of measured buoy data used in comparison of ERA5 data along with
2geographical positions and the water depth

Location		Wave buoy		ERA5		Period	of
Location	Latitude Longitude	Water depth (m)	Distance from coast (km)	Latitude Longitude	Water depth (m)	Period	of validation
off Ratnagiri, eastern Arabian Sea	16.980° N; 73.258° E	13	2.0	17.10° N; 73.20° E	47	1 January 2015 to 31 December 2015	
off Karwar, eastern Arabian Sea	14.822° N, 74.052° E	15	5.0	14.70° N; 73.80° E	48	1 January 2014 to 31 December 2014	
off Puducherry, western Bay of Bengal	11.925° N; 79.851° E	12	2.0	12.00° N; 80.10° E	159	1 January 2010 to 31 December 2010	
off Gangavaram, western Bay of Bengal	17.632° N; 83.265° E	18	2.0	17.70° N; 83.40° E	59	1 January 2010 to 31 December 2010	
off Gopalpur, western Bay of Bengal	19.282° N; 84.964° E	15	1.5	19.20° N; 85.20° E	97	1 January 2015 to 31 December 2015 9 October 2013 to 14 October 2013	

3

4Table 2. Comparison statistics of ERA5 maximum wave height with buoy data

5

Location	Number of data	Buoy			ERA5			R	RMSE (m)	Bias (m)	SI
		mean (m)	maximum (m)	H_{\max}/H_s	mean (m)	maximum (m)	H_{\max}/H_s				
Ratnagiri	8756	1.63	8.60	1.72	1.92	7.60	1.88	0.97	0.40	0.29	0.15
Karwar	8642	1.65	6.97	1.72	2.20	6.53	1.89	0.96	0.70	0.55	0.19
Puducherry	8759	1.07	4.75	1.73	1.65	5.40	1.90	0.81	0.67	0.58	0.21
Gangavaram	8539	1.55	5.24	1.72	2.05	5.42	1.89	0.88	0.63	0.50	0.19
Gopalpur	8759	1.52	4.65	1.71	1.95	5.82	1.89	0.91	0.52	0.43	0.15
Ratnagiri - high waves	744	3.54	8.60	1.67	4.04	7.60	1.84	0.95	0.69	0.50	0.14
Gopalpur - tropical cyclone	330	2.92	13.50	1.67	3.34	12.95	1.88	0.97	0.84	0.43	0.25

Table 3. The maximum value of annual average and maximum wave height during 1979 to 2018 and the date of occurrence along with water depth of the locations studied

Location	Position	Maximum value of annual average H_{max} (m)	Maximum value of H_{max} (m)	Date on which maximum value occurred	water depth (m)	% time H_{max}	
						> 4m	> 8m
1	22.50° N; 68.25° E	2.71	11.58	20 May 1999 (Cyclonic Storm ARB01)	63	18.35	0.04
2	21.00° N; 69.50° E	2.90	15.99	8 June 1998 (Cyclonic Storm ARB 02)	65	19.82	0.17
3	19.50° N; 71.25° E	2.81	13.43	18 June 1996 (Cyclonic Storm ARB 01)	75	18.28	0.14
4	18.00° N; 72.00° E	2.91	11.67	18 June 1996 (Cyclonic Storm ARB 01)	47	18.83	0.18
5	16.50° N; 72.75° E	2.83	10.90	17 June 1996 (Cyclonic Storm ARB 01)	68	18.07	0.16
6	15.00° N; 73.50° E	2.62	10.17	23 July 1989 (Cyclonic Storm BOB 04)	75	15.73	0.09
7	13.50° N; 73.50° E	2.78	10.80	17 June 1996 (Cyclonic Storm ARB 01)	80	17.88	0.12
8	12.00° N; 74.50° E	2.47	9.04	7 June 2000	129	10.47	0.01
9	10.50° N; 75.75° E	2.01	7.67	6 May 2004 (Cyclonic Storm ARB01)	46	1.42	-
10	09.00° N; 76.00° E	2.59	8.10	6 May 2004 (Cyclonic Storm ARB01)	90	8.87	0.00
11	07.75° N; 77.25° E	3.11	6.72	13 Nov 1992 (Cyclonic Storm BOB07)	61	14.61	-
12	10.50° N; 80.25° E	1.83	7.31	3 Dec 1993 (Cyclonic Storm BoB02)	104	0.36	-
13	12.00° N; 80.00° E	1.79	10.44	30 Dec 2011 (TC Thane)	27	0.37	0.01
14	13.50° N; 80.50° E	1.89	11.88	12 Dec 2016 (TC Vardah)	90	0.49	0.02
15	15.00° N, 80.25° E	1.67	12.26	12 May 1979 (Category 2 TC)	49	0.34	0.01
16	16.75° N, 82.50° E	2.05	9.47	12 May 1979 (Category 2 TC)	99	0.85	0.02
17	18.50° N; 84.50° E	2.38	12.67	12 Oct 2014 (TC Hudhud)	41	3.29	0.03
18	20.00° N; 86.75° E	2.41	12.49	12 Oct 2013 (TC Phailin)	58	4.81	0.05
19	21.00° N; 89.00° E	2.67	17.94	25 May 2009 (TC Aila)	75	10.59	0.13

9Table 4. Mean and trend value of annual maximum, 99th, 95th, 90th percentile and annual mean 10maximum wave height at different locations during 1979 to 2018. Last two columns shows the 11trend value of annual mean and annual maximum H_s

Location	Annual maximum		99 th percentile		95 th percentile		90 th percentile		Annual mean		Annual mean H _s	Annual maximum H _s
	Mean (m)	Trend (cm/yr)	Mean (m)	Trend (cm/yr)	Mean (m)	Trend (cm/yr)	Mean (m)	Trend (cm/yr)	Mean (m)	Trend (cm/yr)	Trend (cm/yr)	Trend (cm/yr)
1	7.76	-0.1	6.51	0.3	5.48	1.2	4.81	0.9	2.55	0.2	0.1	0.1
2	8.38	-0.3	6.98	0.3	5.90	1.2	5.15	1.0	2.67	0.2	0.1	-0.1
3	8.30	-0.2	6.81	0.9	5.69	1.1	4.98	0.8	2.59	0.3	0.2	0.0
4	8.25	0.1	6.90	1.2	5.78	0.9	5.04	0.6	2.66	0.2	0.1	0.2
5	8.04	0.9	6.83	1.2	5.69	0.8	4.91	0.6	2.60	0.2	0.1	0.6
6	7.56	0.6	6.42	1.2	5.34	0.6	4.60	0.5	2.45	0.2	0.1	0.4
7	7.84	1.2	6.62	1.4	5.55	0.8	4.79	0.8	2.61	0.3	0.2	0.7
8	6.48	1.5	5.47	1.0	4.60	0.8	4.04	0.8	2.33	0.2	0.1	0.8
9	4.95	2.0	4.07	1.0	3.44	0.8	3.10	0.8	1.87	0.3	0.2	1.1
10	5.94	1.9	5.02	1.4	4.34	1.1	3.93	1.1	2.40	0.4	0.2	1.1
11	5.84	0.7	5.07	0.4	4.53	0.6	4.21	0.6	2.94	0.3	0.2	0.5
12	4.90	1.4	3.50	0.6	2.88	0.4	2.58	0.3	1.72	0.2	0.1	0.8
13	5.25	3.2	3.38	0.9	2.67	0.3	2.38	0.2	1.69	0.2	0.1	1.7
14	5.76	4.2	3.50	0.5	2.64	0.2	2.38	0.2	1.77	0.2	0.1	2.2
15	5.24	-1.1	3.17	-0.1	2.37	-0.1	2.16	-0.1	1.60	0.0	0.0	-0.5
16	5.66	1.5	3.92	0.1	3.08	0.3	2.77	0.3	1.94	0.1	0.1	0.7
17	6.98	4.6	4.74	0.6	3.75	0.8	3.34	0.6	2.24	0.2	0.1	2.4
18	7.36	0.4	5.08	0.7	3.98	0.5	3.53	0.4	2.27	0.2	0.1	0.3
19	8.91	-1.7	6.09	0.6	4.63	0.3	4.04	0.6	2.49	0.1	0.1	-0.8

13**Table 5.** Root Mean Square Error values for the three theoretical distributions with wave height
 14distribution for all locations

Location	Root Mean Square Error (%)		
	Rayleigh	Log-normal	GEV
1	1.44	0.93	0.96
2	1.51	1.04	0.87
3	1.63	1.13	0.86
4	1.89	1.35	0.96
5	2.01	1.46	1.05
6	2.23	1.70	1.28
7	2.17	1.66	1.20
8	2.16	1.60	1.24
9	2.31	1.66	1.50
10	1.71	1.26	1.25
11	1.60	0.79	0.81
12	1.66	0.65	0.70
13	2.26	0.22	0.12
14	2.43	0.31	0.33
15	2.45	0.23	0.26
16	1.79	0.48	0.43
17	1.13	0.48	0.48
18	0.88	0.66	0.68
19	0.69	0.57	0.63

15

16

17Figure Captions

18Figure 1. Locations considered in the study are 1 to 19. Waverider buoy locations are shown as
19triangle. Colour shade is water depth in metres

20Figure 2. Scatter plots of maximum wave height from buoy against the ERA5 at different
21locations; a) Ratnagiri in 2015, b) Karwar in 2014, c) Puducherry in 2010, d) Gangavaram in
222010, e) Gopalpur in 2015. Solid line is the exact match line and dotted lines are 10% deviation
23from the exact match line

24Figure 3. Time series plots of maximum wave height from ERA5 and buoy measured a) at
25Ratnagiri during 4 June 2015 to 4 July 2015, b) at Gopalpur during tropical cyclone Phailin (9-14
26October 2013)

27Figure 4. Spatial distribution of monthly average maximum wave height in different months.
28Data from 1979 to 2018 with temporal resolution of 1 hour and spatial resolution of 31 km is
29used

30Figure 5. Month versus year plots of maximum wave height at different locations

31Figure 6. Daily variation in maximum wave height in 2018 at different locations

32Figure 7. Monthly average maximum wave height at different locations in different months

33Figure 8. Plots of mean, median, 25th percentile, 75th percentile, 90th percentile, 95th percentile,
3499th percentile of maximum wave height along with the standard deviation of annual mean from
351979 to 2018 at 19 locations

36Figure 9. Time series plots of annual maximum value of maximum wave height from 1979 to
372018 at the 19 locations

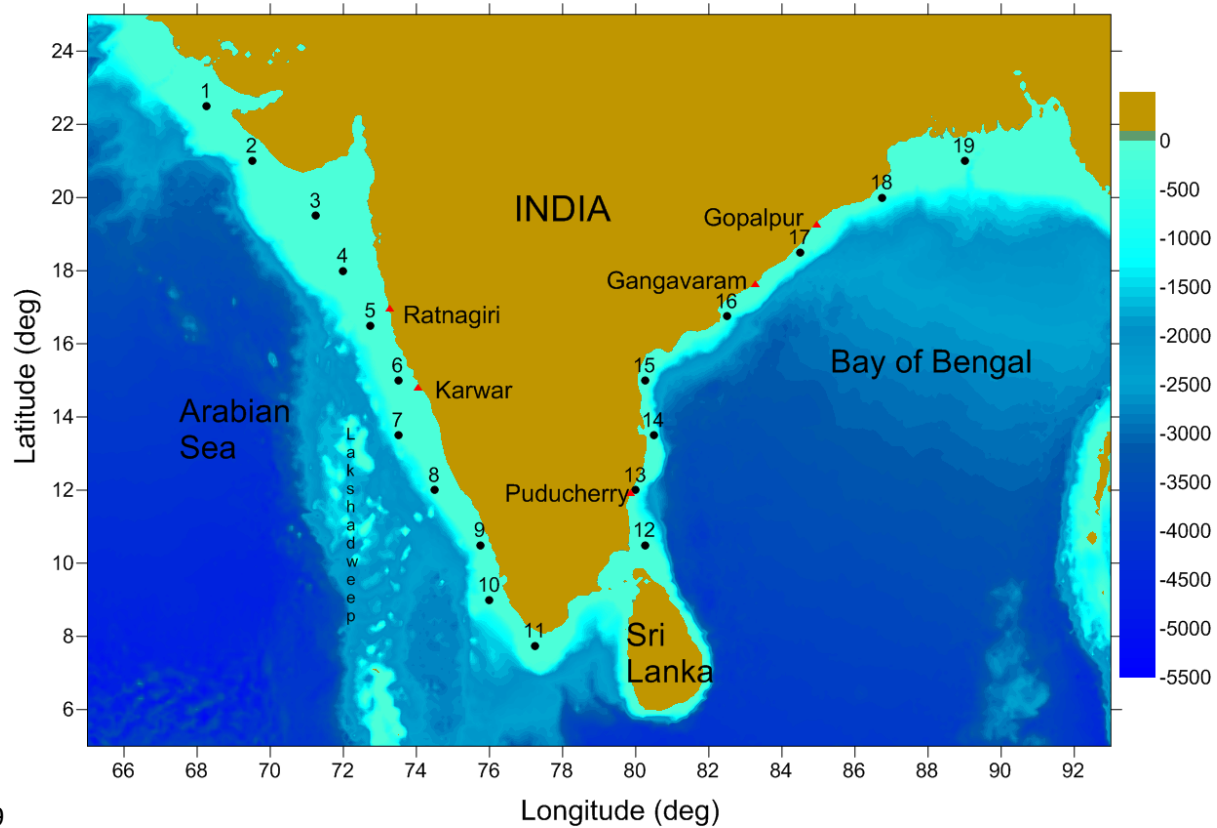
38Figure 10. Time series plots of annual mean value of maximum wave height from 1979 to 2018
39at the 19 locations. The trend for the period 1979 to 2018, 1979 to 1991 and 1992 to 2018 are
40also presented

41Figure 11. Histogram of maximum wave height and the corresponding Rayleigh, long-normal
42and Generalised Extreme Value distribution at different locations

43Figure 12. Seasonal and annual anomaly in maximum wave height at different locations. a)
44February-May, b) June-September, c) October-January and d) January-December

45Figure 13. Correlation coefficient between a) seasonal maximum wave height anomaly and
46Oceanic Niño Index (ONI) in three different seasons and b) maximum wave height anomaly in
47October and dipole mode index (DMI)

48



49

50

51 Figure 1. Locations considered in the study are 1 to 19. Waverider buoy locations are shown as triangle. Colour shade is water depth
52 in metres

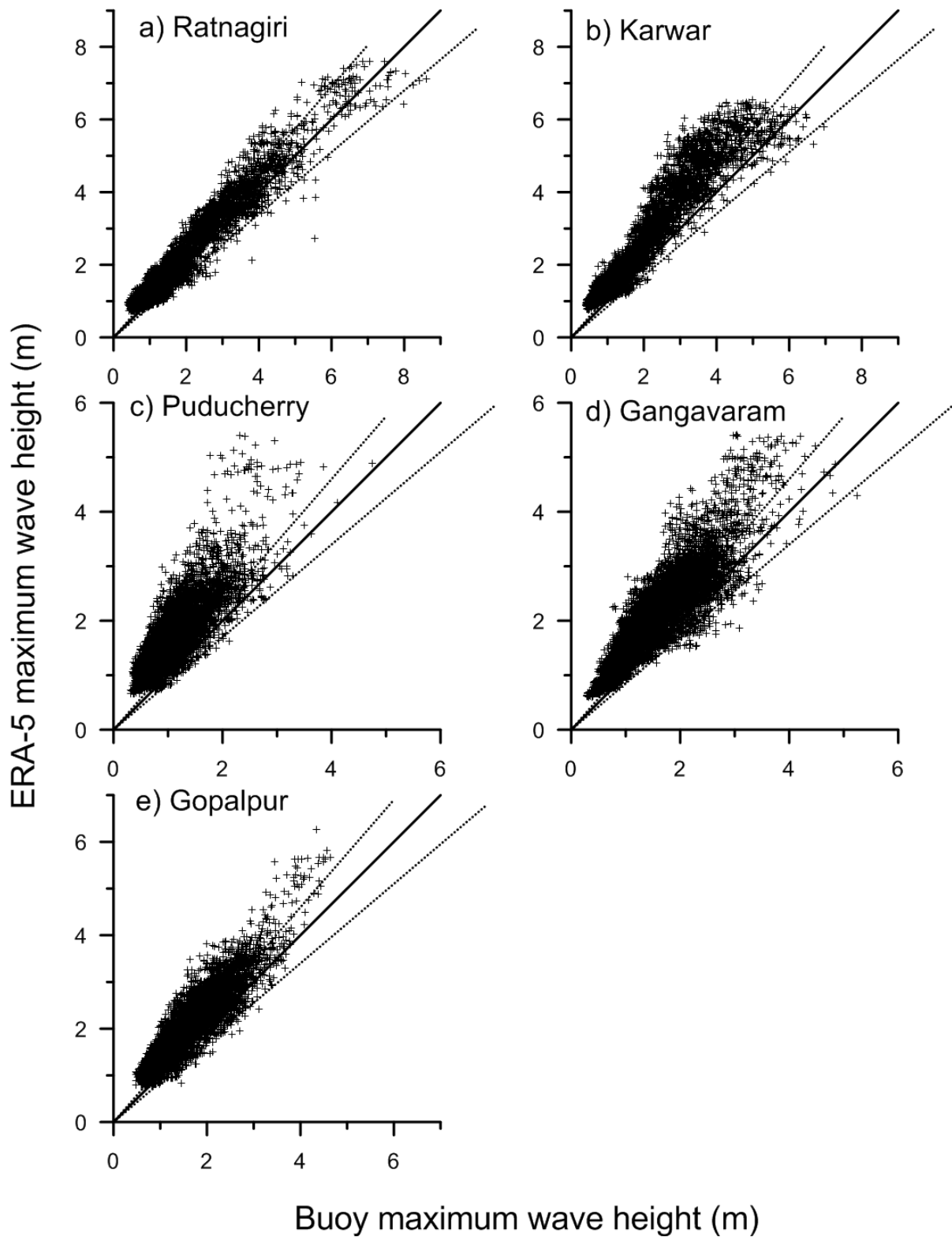


Figure 2. Scatter plots of maximum wave height from buoy against the ERA5 at different locations; a) Ratnagiri in 2015, b) Karwar in 2014, c) Puducherry in 2010, d) Gangavaram in 2010, e) Gopalpur in 2015. Solid line is the exact match line and dotted lines are 10% deviation from the exact match line

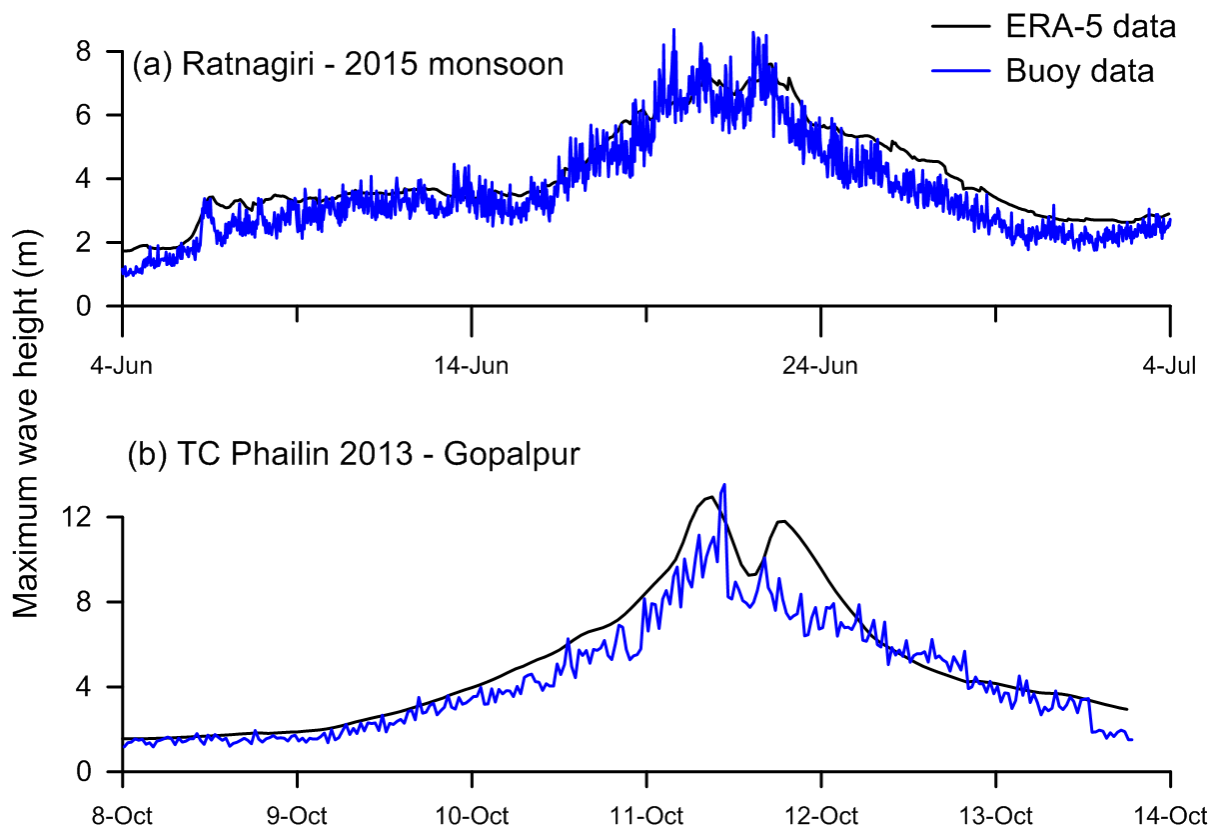


Figure 3. Time series plots of maximum wave height from ERA5 and buoy measured a) at Ratnagiri during 4 June 2015 to 4 July 2015, b) at Gopalpur during tropical cyclone Phailin (9-14 October 2013)

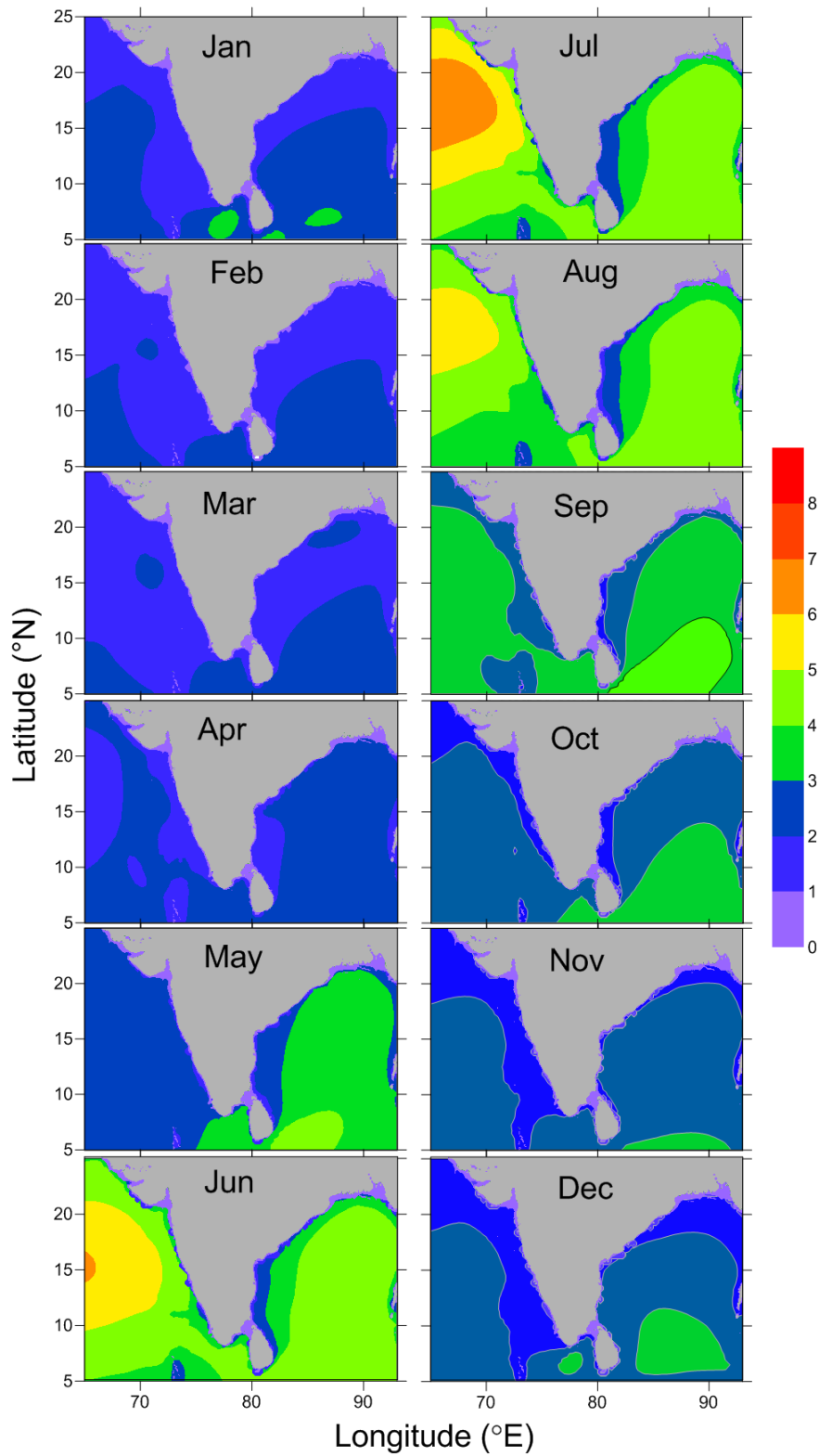


Figure 4. Spatial distribution of monthly average maximum wave height in different months. Data from 1979 to 2018 with temporal resolution of 1 hour and spatial resolution of 31 km is used

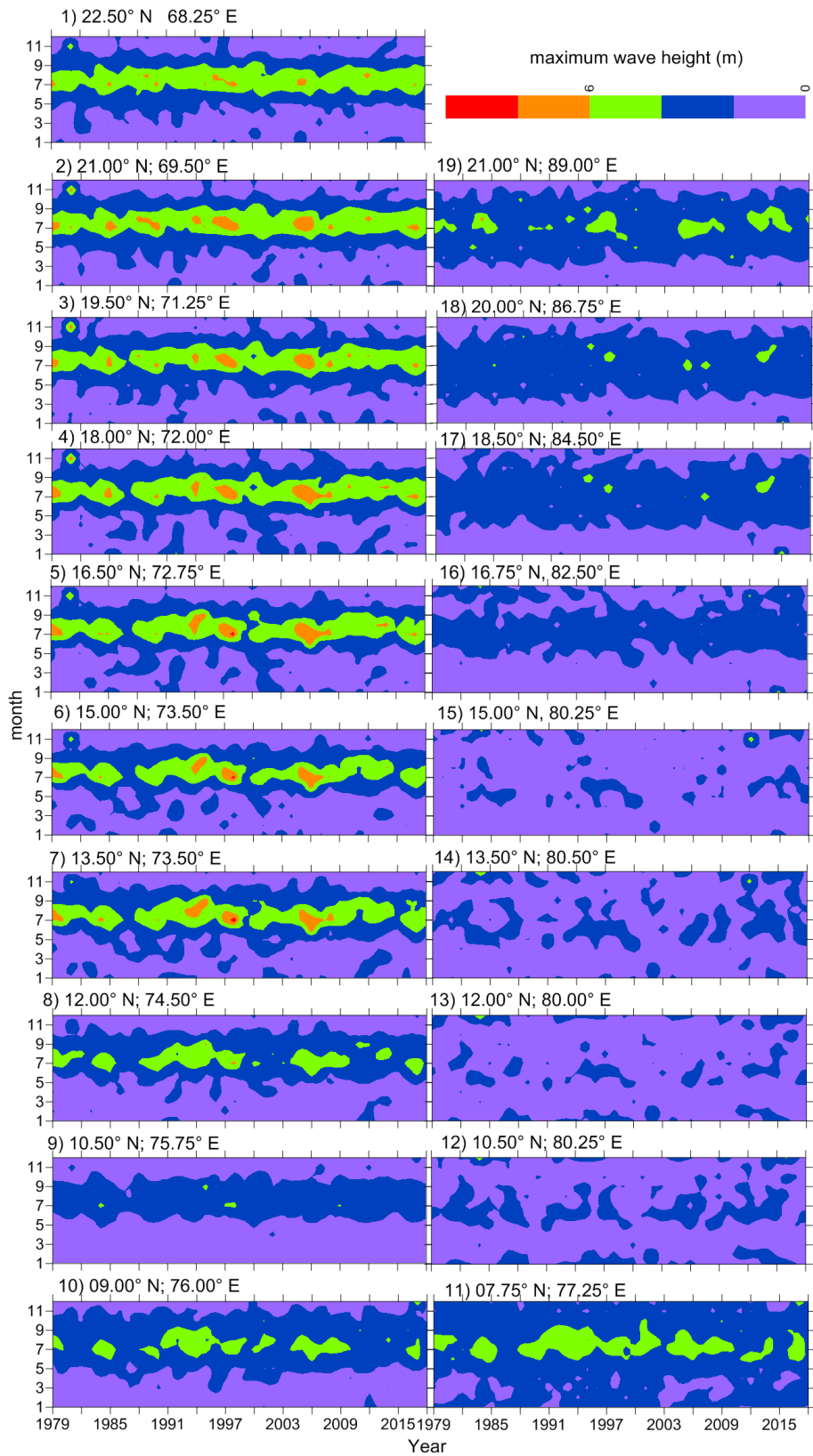


Figure 5. Month versus year plots of maximum wave height at different locations

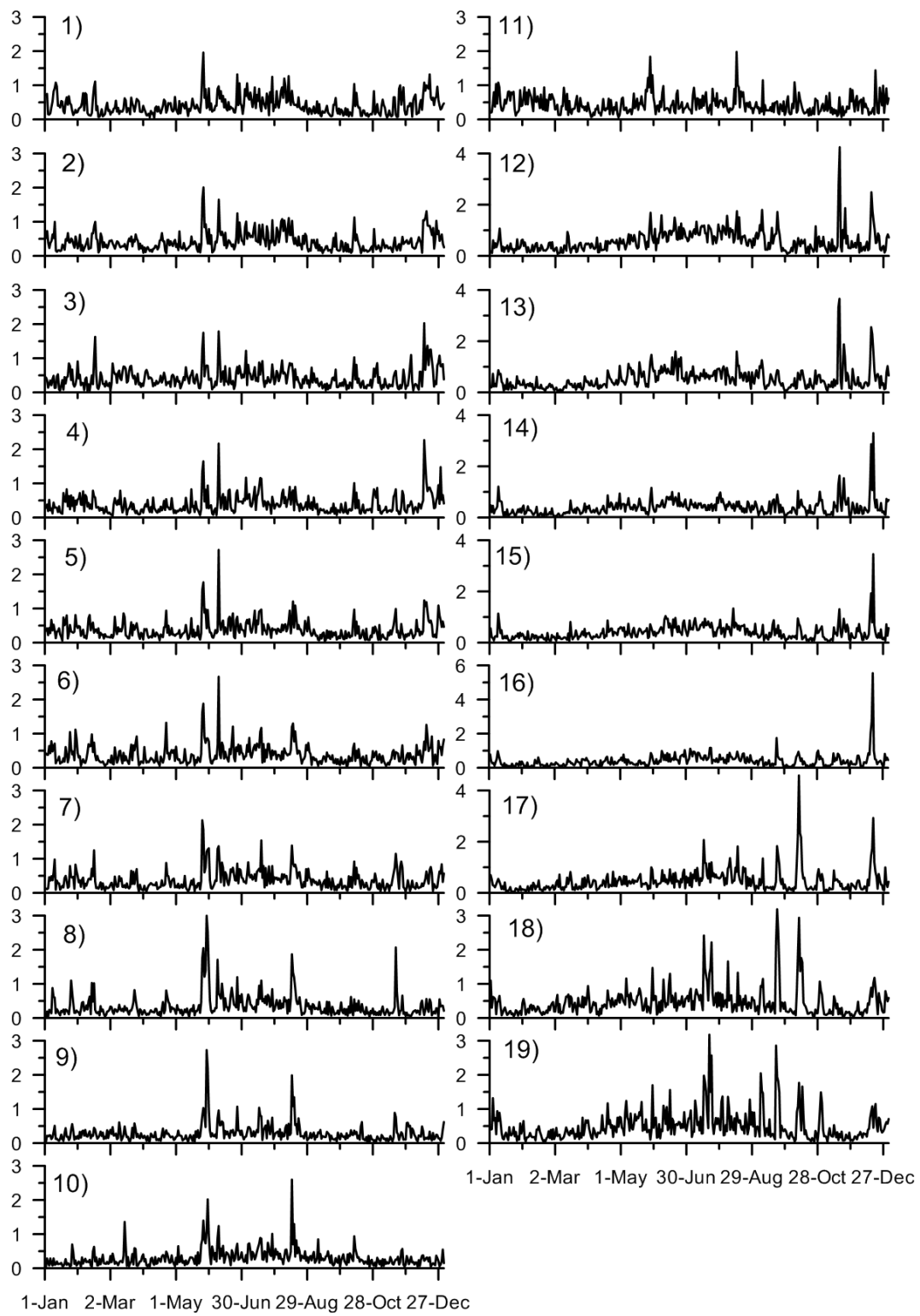


Figure 6. Daily variation in maximum wave height in 2018 at different locations

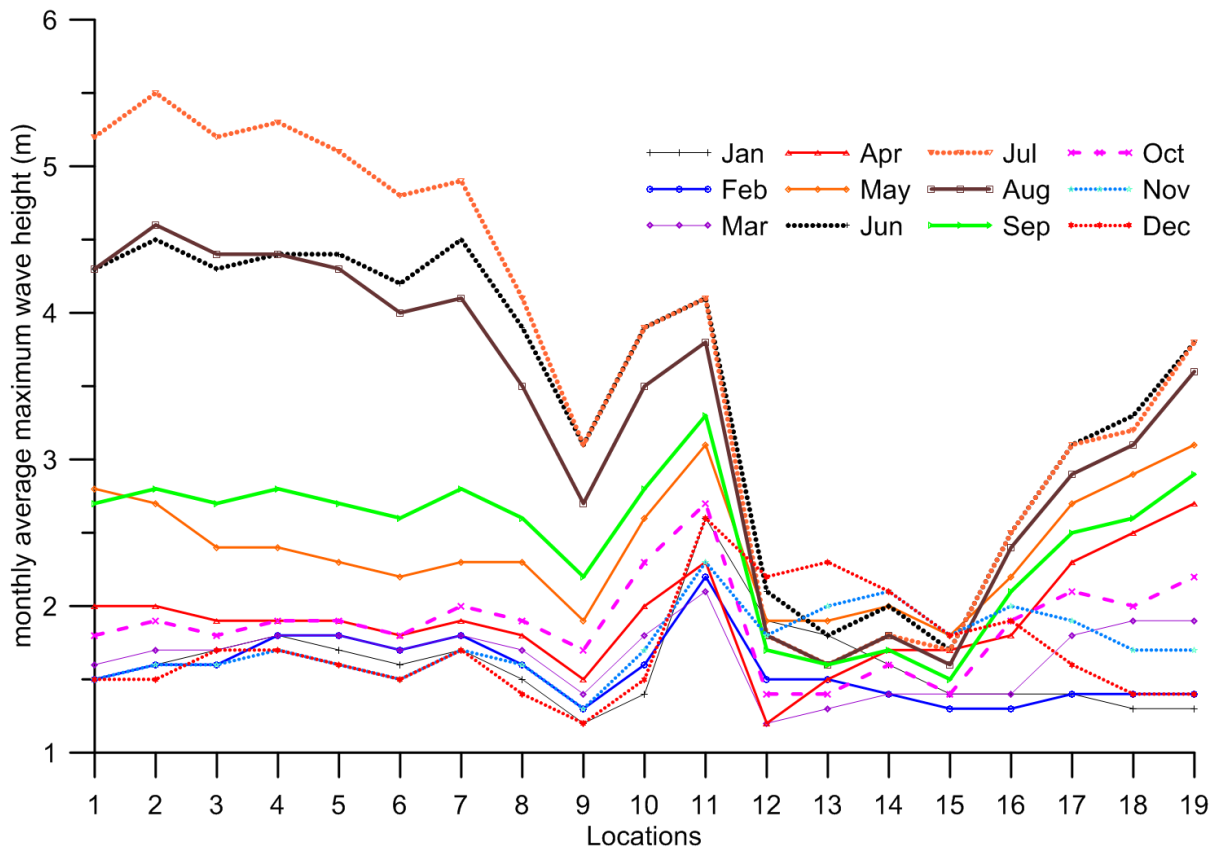


Figure 7. Monthly average maximum wave height at different locations in different months

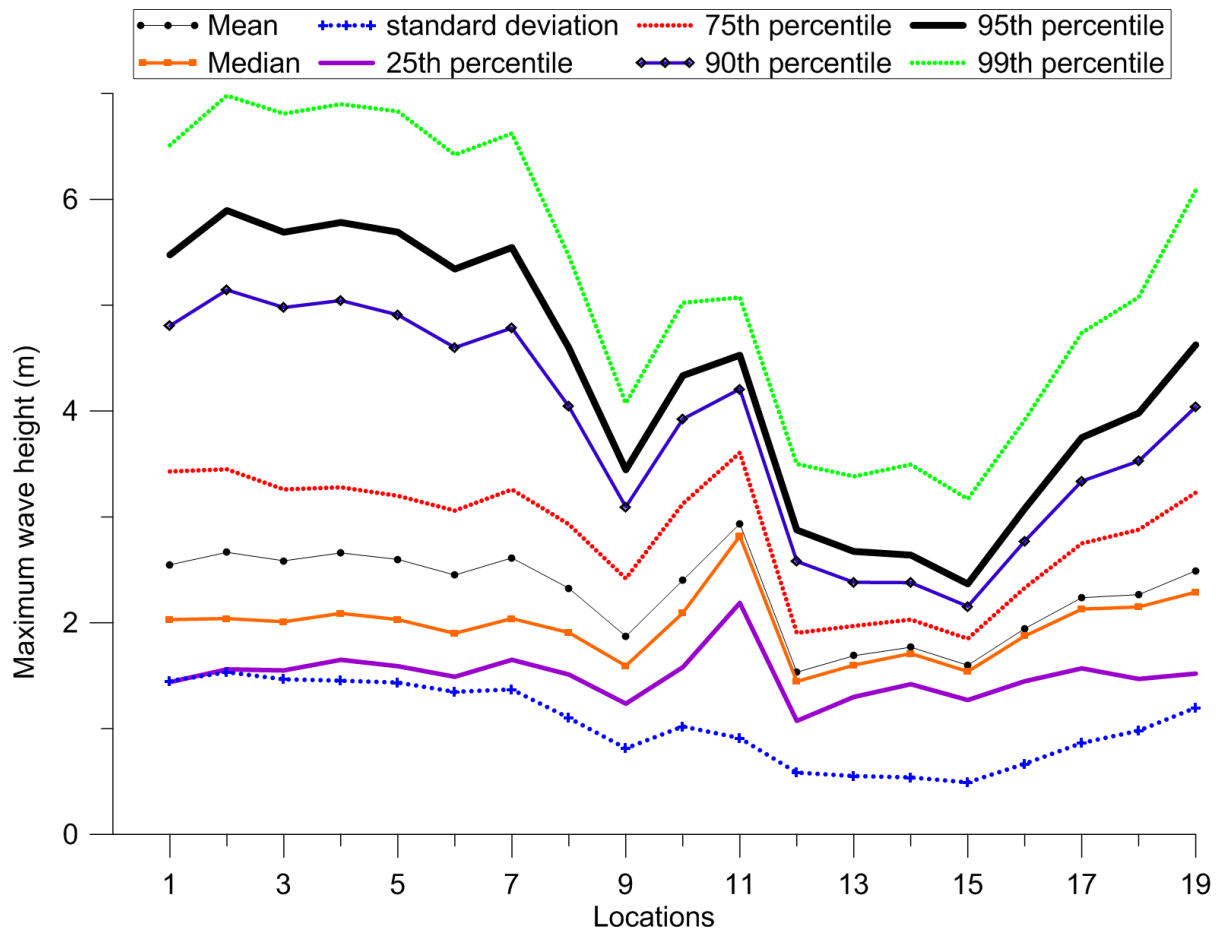


Figure 8. Plots of mean, median, 25th percentile, 75th percentile, 90th percentile, 95th percentile, 99th percentile of maximum wave height along with the standard deviation of annual mean from 1979 to 2018 at 19 locations

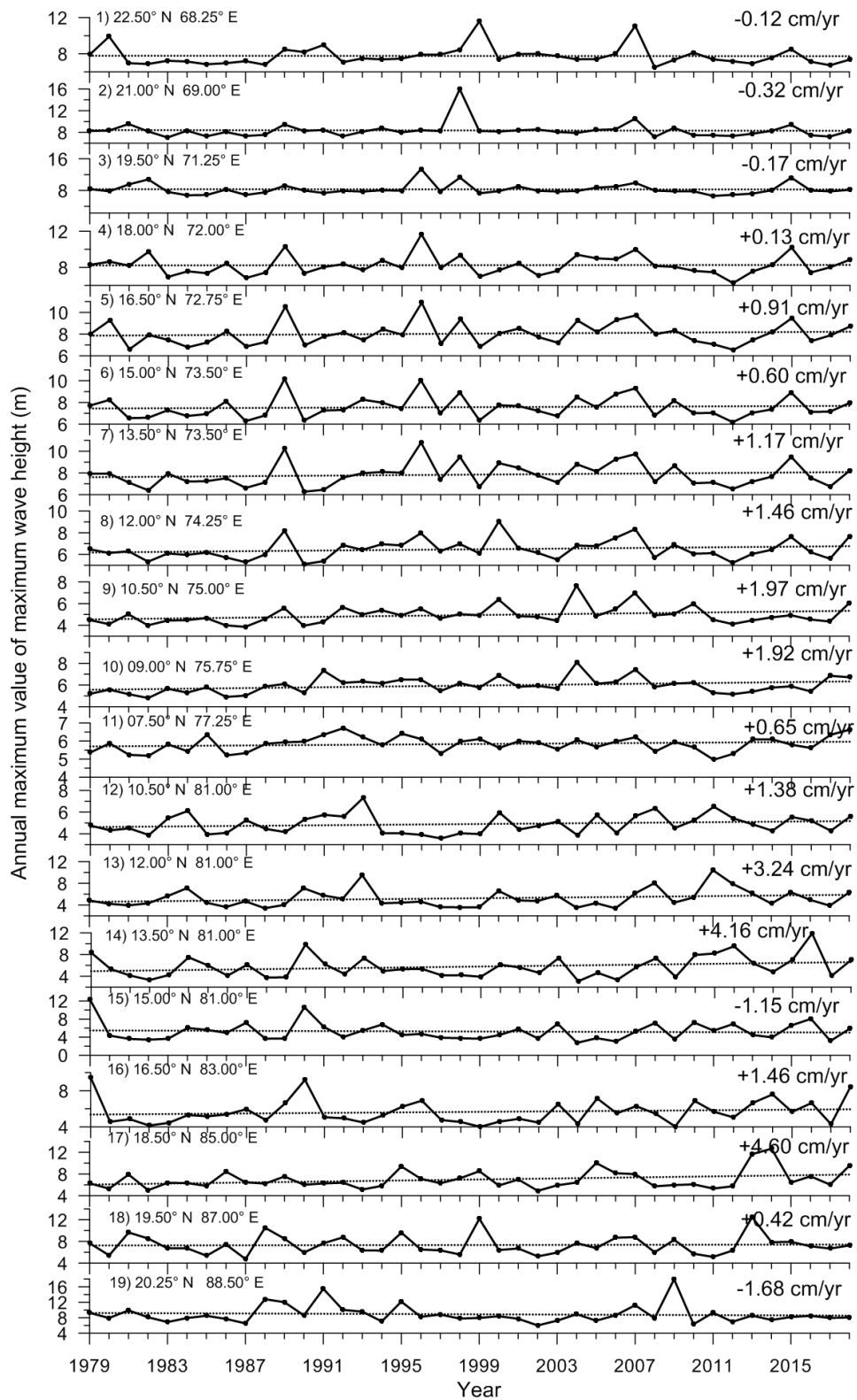


Figure 9. Time series plots of annual maximum value of maximum wave height from 1979 to 2018 at the 19 locations

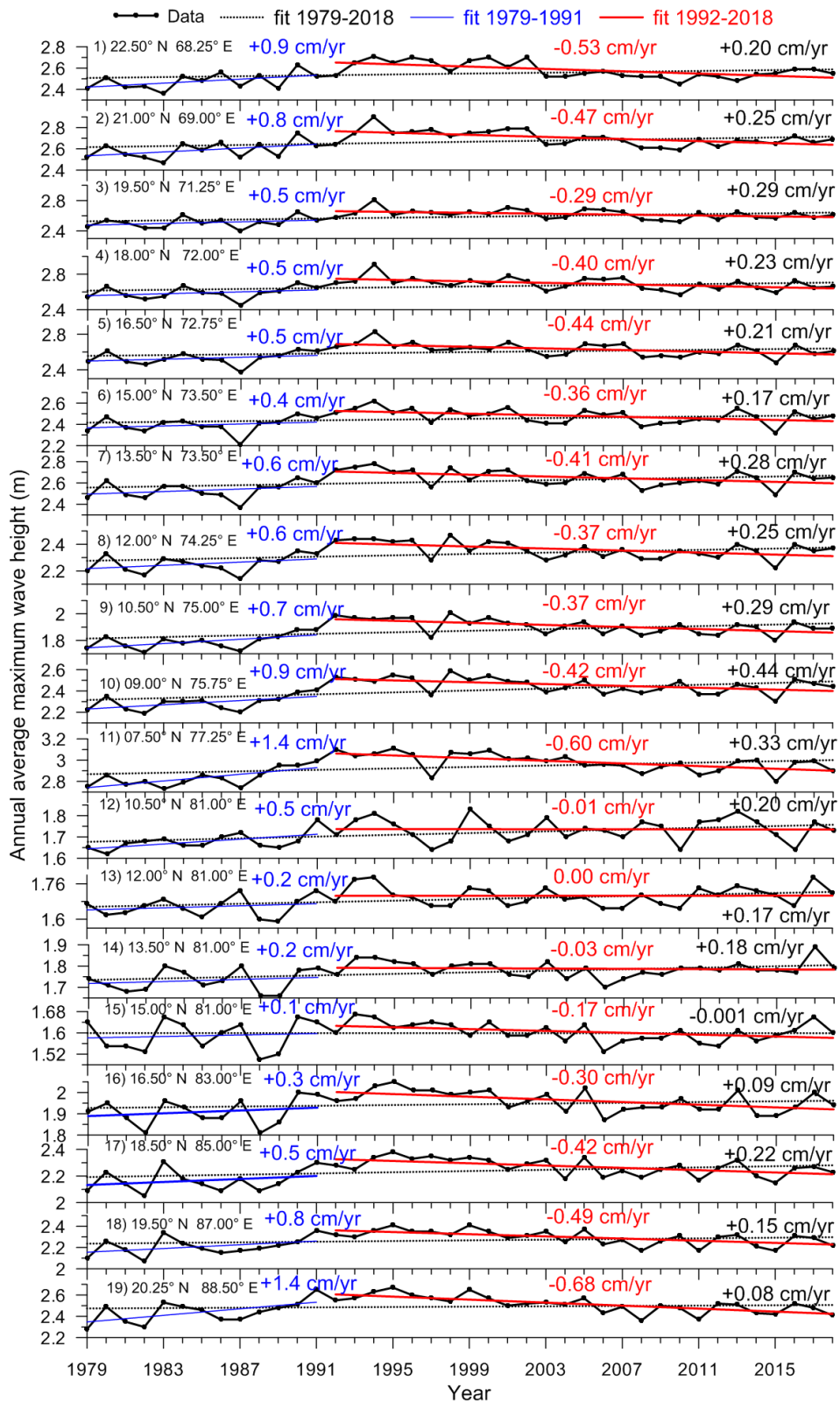


Figure 10. Time series plots of annual mean value of maximum wave height from 1979 to 2018 at the 19 locations. The trend for the period 1979 to 2018, 1979 to 1991 and 1992 to 2018 are also presented

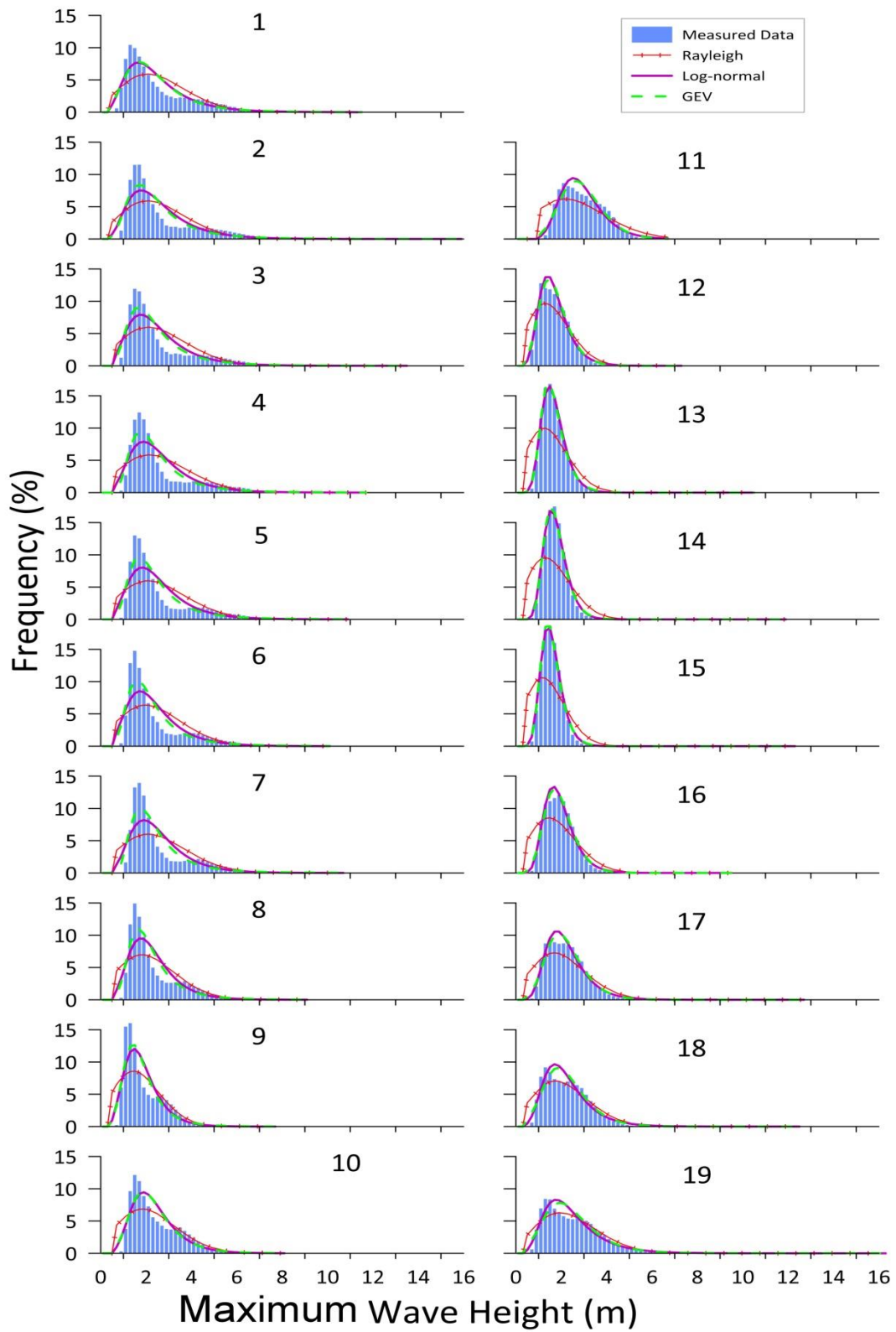


Figure 11. Histogram of maximum wave height and the corresponding Rayleigh, long-normal and Generalised Extreme Value distribution at different locations

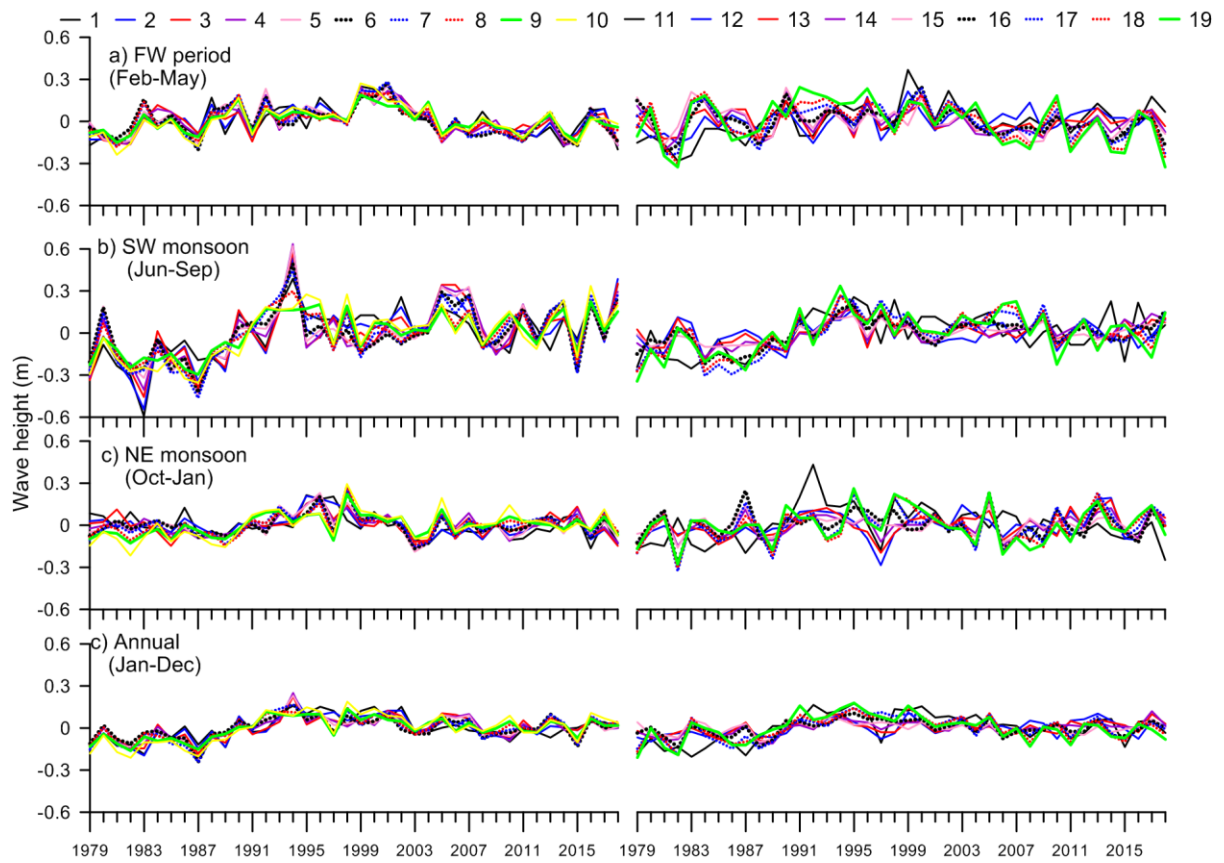


Figure 12. Seasonal and annual anomaly in maximum wave height at different locations. a) February-May, b) June-September, c) October-January and d) January-December

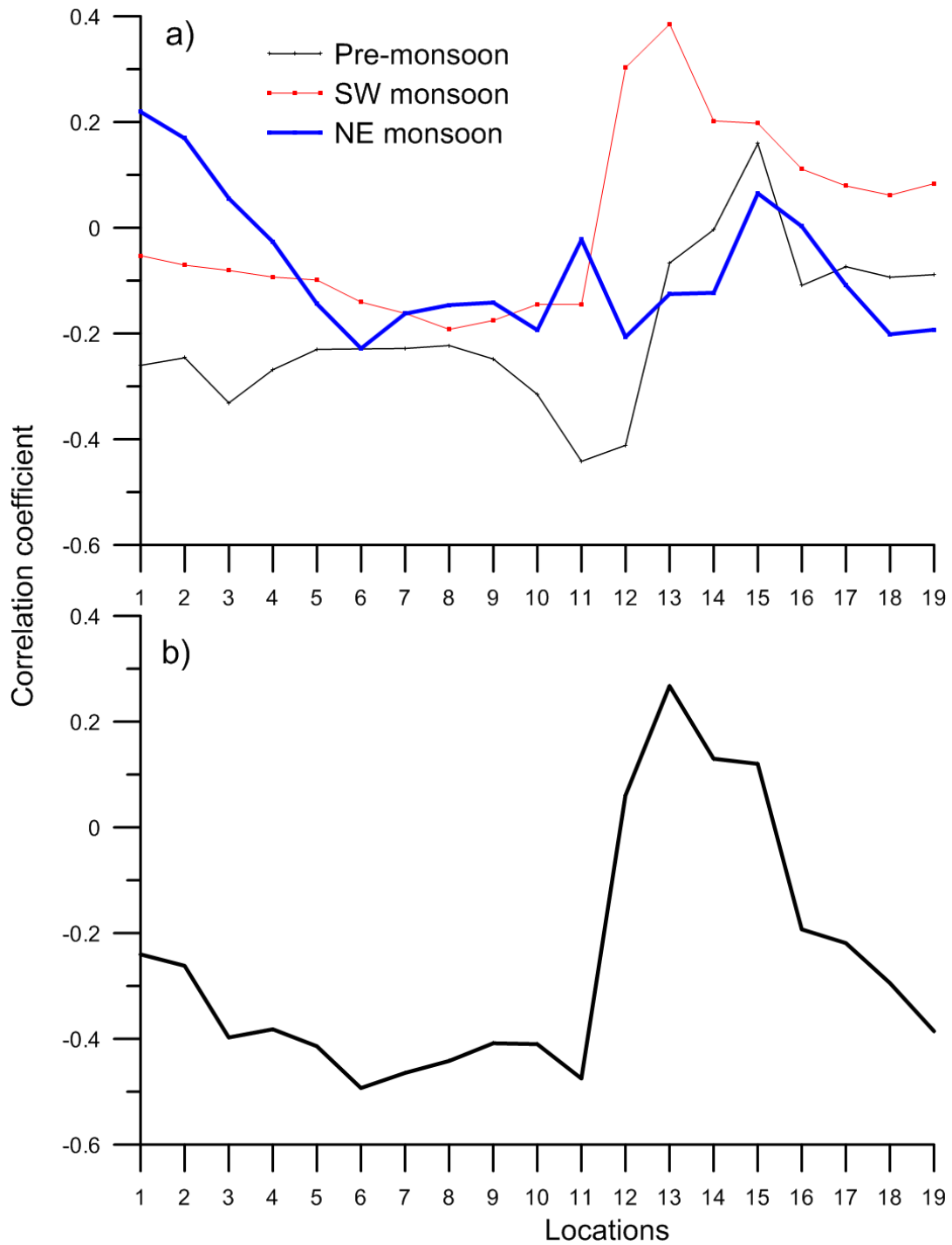


Figure 13. Correlation coefficient between a) seasonal maximum wave height anomaly and Oceanic Niño Index (ONI) in three different seasons and b) maximum wave height anomaly in October and dipole mode index (DMI)